

GW170104 and the origin of heavy, low-spin binary black holes via classical isolated binary evolution

K. Belczynski^{1*}, J. Klencki¹, G. Meynet⁴, C. L. Fryer⁵, D. A. Brown^{2,3}, M. Chruslinska¹, W. Gladysz¹, R. O’Shaughnessy⁶, T. Bulik¹, E. Berti^{7,8}, D.E. Holz⁹, D. Gerosa^{10**}, M. Giersz¹¹, S. Ekstrom⁴, C. Georgy⁴, A. Askar¹¹, and J.-P. Lasota^{11,12}

¹ Astronomical Observatory, Warsaw University, Al. Ujazdowskie 4, 00-478 Warsaw, Poland

² Department of Physics, Syracuse University, Syracuse NY 13224

³ Kavli Institute of Theoretical Physics, UC Santa Barbara, CA, USA

⁴ Department of Astronomy, University of Geneva, Chemin des Maillettes 51, 1290 Versoix, Switzerland

⁵ CCS-2, MSD409, Los Alamos National Laboratory, Los Alamos, NM 87545, USA

⁶ Center for Computational Relativity and Gravitation, Rochester Institute of Technology, Rochester, New York 14623, USA

⁷ Department of Physics and Astronomy, The University of Mississippi, University, MS 38677, USA

⁸ CENTRA, Departamento de Física, Instituto Superior Técnico, Universidade de Lisboa, Avenida Rovisco Pais 1, 1049 Lisboa, Portugal

⁹ Enrico Fermi Institute, Department of Physics, Department of Astronomy and Astrophysics, and Kavli Institute for Cosmological Physics, University of Chicago, Chicago, IL 60637, USA

¹⁰ TAPIR 350-17, California Institute of Technology, 1200 E. California Blvd., Pasadena, California 91125, USA

¹¹ Nicolaus Copernicus Astronomical Centre, Polish Academy of Sciences, ul. Bartycka 18, 00-716 Warsaw, Poland

¹² Institut d’Astrophysique de Paris, CNRS et Sorbonne Universités, UPMC Paris 06, UMR 7095, 98bis Bd Arago, 75014 Paris, France

Received June 21, 2017; accepted ???

ABSTRACT

Context. The Advanced Laser Interferometer Gravitational-wave Observatory (LIGO) has observed four binary black hole mergers thus far. The effective spin of GW170104 has an 82% probability of being negative, which would indicate spin-orbit misalignment. It has been suggested that LIGO’s detections favor a population of binaries with frequent and significant spin-orbit misalignment, hence supporting dynamical formation over classical isolated binary evolution. However, it is also well known that massive stars can have efficient transport of angular momentum within the star and have strong winds that carry away substantial angular momentum. The progenitors of the heaviest stellar-mass black holes ($M > 30 M_{\odot}$) are expected to efficiently reduce their angular momentum, producing black holes with low spin. Low black hole natal spins for these heaviest black holes would be consistent with existing LIGO constraints on black hole spins.

Aims. We use a physically motivated model for black hole natal spins to track the spins in a simulated population of binary black holes produced by classical isolated binary evolution. This allows us to determine whether the black hole mergers detected by LIGO would be naturally produced by classical isolated binary evolution, or if other formation channels are required to explain LIGO’s observations.

Methods. A stellar evolution model that incorporates rotation (the Geneva code) is used to determine the natal spins of the black holes produced by core collapse. These natal spins are incorporated into our population synthesis code (StarTrack) which follows the evolution of Population I/II stars across cosmic time and predicts the binary black hole population in the universe.

Results. Our model produces a binary black hole population that is consistent with the observed LIGO population. In particular, it produces systems that are consistent with the measured properties of GW170104; total mass, mass ratio, effective spin and the overall binary black hole merger rate. Neither strong natal black hole kicks nor dynamical interactions are required to recover GW170104.

Conclusions. Classical evolution of isolated binary systems is consistent with the population of binary black holes observed by LIGO. LIGO’s observations do not provide evidence for dynamical formation over classical isolated binary formation and it is not yet possible to establish the evolutionary channel through which GW170104 was formed.

Key words. Stars: massive – Black-hole physics – Gravitational waves

1. Introduction

Advanced LIGO has reported the observation of four binary black hole mergers: GW150914, LVT151012, GW151226, and GW170104 (Abbott et al. 2016d,c,a; Abbott et al. 2017b). All of these binaries, except GW151226, contain “heavy” black holes

with component masses $> 20 M_{\odot}$. These black hole masses are consistent with formation by isolated binary evolution of stars with metallicities $< 10\% Z_{\odot}$ and initial masses in the range 40–100 M_{\odot} interacting through mass transfer and a common envelope phase (Belczynski et al. 2010a, 2016b) and were predicted to be the first LIGO sources (Belczynski et al. 2010b).

The spins of the black holes also provide important information on their formation. However, the effect of spin is sub-

* chrisbelczynski@gmail.com

** Einstein Fellow

dominant in the gravitational waveform and it is more difficult to measure than mass. The waveform is most sensitive to the binary’s effective spin

$$\chi_{\text{eff}} = \frac{M_{\text{BH}1} a_{\text{spin}1} \cos \Theta_1 + M_{\text{BH}2} a_{\text{spin}2} \cos \Theta_2}{M_{\text{BH}1} + M_{\text{BH}2}} \quad (1)$$

with $a_{\text{spin}1,2}$ the black hole spin magnitudes and $\Theta_{1,2}$ the angles between the binary’s angular momentum direction and the black hole’s spin direction. The dimensionless BH spin magnitude is defined as:

$$a_{\text{spin}} = c J_{\text{BH}} / (G M_{\text{BH}}^2) \quad (2)$$

where c is the speed of light, G is the gravitational constant, and M_{BH} , J_{BH} are the mass and angular momentum of the BH, respectively.

All of the LIGO-observed binaries are consistent with low effective spins with $|\chi_{\text{eff}}| \lesssim 0.4$ at the 90% credible level Abbott et al. (2016a); Abbott et al. (2017b). For example, for GW170104 Abbott et al. (2017b) report that $\chi_{\text{eff}} = -0.12^{+0.21}_{-0.30}$ at the 90% credible level. Only GW151226 has an effective spin inconsistent with zero, implying that one component black hole has a spin magnitude of $a_{\text{spin}} \geq 0.2$ at the 99% credible level (Abbott et al. 2016c). All other binaries are consistent with either positive or negative effective spins (Abbott et al. 2016a; Abbott et al. 2017b). Abbott et al. (2017b) report that GW170104 has a preferentially negative effective spin—indicative of spin-orbit misalignment of at least one component black hole—with an 82% probability that $\chi_{\text{eff}} < 0$. Abbott et al. (2017b) state that these observations are consistent with both dynamical assembly and isolated binary evolution, provided that the positive orbit-aligned spins are small. If the black hole spins are large ($a_{\text{spin}1,2} > 0.2$), Abbott et al. (2017b) state that the LIGO observations suggest a population of binaries with spin-orbit misalignment. A population of binary black holes dominated by misaligned spins would favor a dynamical formation scenario over classical isolated binary evolution. However, black hole spin magnitudes in GW170104 are not constrained, and in particular they can be zero (Abbott et al. 2017b).

Previous work to model the population of compact-object mergers produced by classical isolated binary evolution has not carefully explored the distribution of expected spins. In this paper, we use a physical model of the black hole spin evolution that incorporates detailed stellar evolution of rotating progenitor stars through core collapse (natal black hole spin) and simulations with accretion and spin-up during the binary evolution (final black hole spin). We argue that the most massive black holes will be born with slow natal spins, which are at best modestly increased by accretion over their lifetime. By incorporating this information into our binary evolution and synthetic universe simulations, we demonstrate that the population of binary black holes observed by LIGO can be produced by classical isolated binary evolution. The observed population is well explained by small natal spins for massive black holes that do not significantly increase during binary evolution. Dynamical formation channels are not necessary to produce the observed distribution of effective spins in binary black holes.

To illustrate the uncertainties present in our binary evolution and the impact of these uncertainties on observations, we conduct a limited parameter study focusing on a few key parameters used to characterize the evolution of massive binary stars. We show how different but still physically consistent choices for these parameters can lead to modest but important changes in the distribution of the mass and spin of black holes.

To focus our study on the impact of the natal BH spin distribution, we organize our presentation conservatively, to avoid uncertainties in how the stellar and BH spin orientation changes as the binary evolves. Gerosa et al. (2017, in prep.) will provide a detailed exploration of how BH natal kicks and tides can change the spin-orbit orientations $\Theta_{1,2}$, and thereby influence χ_{eff} . In this work, rather than performing a systematic parameter study on spin-orbit misalignment and realignment mechanisms, for each binary BH-BH merger we calculate $\chi_{\text{eff,max}}$, the value of χ_{eff} calculated assuming perfect spin-orbit alignment:

$$\chi_{\text{eff,max}} = \frac{M_{\text{BH}1} a_{\text{spin}1} + M_{\text{BH}2} a_{\text{spin}2}}{M_{\text{BH}1} + M_{\text{BH}2}}. \quad (3)$$

Equivalently, our results were generated by assuming BHs are negligibly misaligned from (or efficiently realigned with) their orbit. Effectively, we report the maximum value of the effective spin parameter (in respect to black hole tilt angles) in our results. When operative, mis- and re-alignment mechanisms can enable frequent formation of BH-BH binaries with small or negative χ_{eff} (see, e.g. Rodriguez et al. (2016c) and Gerosa et al. 2017, in prep.). Spin-orbit misalignment is also consistent with features of GW151226 (Abbott et al. 2016c; O’Shaughnessy et al. 2017). While these mechanisms can, under suitable assumptions, make isolated binary evolution models easier to reconcile with LIGO’s observations, these misalignment mechanisms are not needed for our calculations to reproduce binaries whose masses and spins (via χ_{eff}) are consistent with all LIGO observations to date.

This paper is organized as follows. In § 2 we describe the evolutionary models performed in this work, emphasizing the differences relative to recent studies with our code *StarTrack* (Belczynski et al. 2016b,a). In § 3 we show how our adopted model can reproduce existing LIGO observations by incorporating a low natal spins that our model predicts for massive black holes. We also perform a small parameter study, to assess how much our predictions might change due to changes in pertinent sub-dominant parameters. In § 4 we discuss our results.

2. Classical Isolated Binary Evolution

2.1. Stellar evolution

We employ the Geneva stellar evolutionary code (Eggenberger et al. 2012; Georgy et al. 2013) to estimate properties of massive stars prior core-collapse. Models for wide range of metallicities are used: $Z = 0.014, 0.002, 0.006, 0.00004$ (Ekström et al. (2012); Georgy et al. (2013); Eggenberger et al. in prep; Groh et al. in prep.) All the models are computed with the same physical ingredients except for the initial chemical composition.

The models have been computed with a modest core-overshooting during the core H- and He-burning phase (the core has been extended beyond the Schwarzschild limit by a length given by 10% the local pressure scale height). Mass loss rates by stellar winds are accounted for (see the above references for the details). The effects of rotation are included according to the theory by Zahn (1992). In these models, the transport of the angular momentum and the mixing of the chemical species in the radiative zones are due to shear instabilities and meridional currents. Shear instabilities are the main driver for the chemical species, while angular momentum is mainly transported by meridional currents. The angular momentum transport by meridional currents mildly couples the core rotation with that of the envelope. Gradients of angular momentum appear during the Main Sequence phase and become stronger and stronger when evolution proceeds. These models are less efficient for removing an-

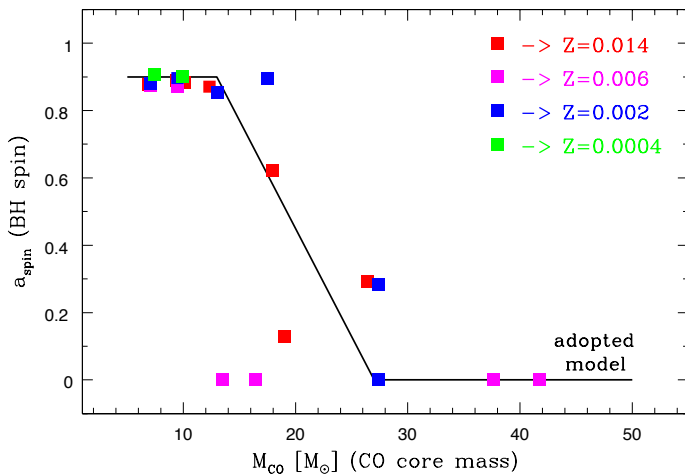


Fig. 1. Magnitude of natal (initial) BH spin as a function of CO core mass of collapsing star. Stellar models at various metallicities (marked with different colors) were obtained with the Geneva evolutionary code with 40% of the critical rotation on ZAMS. The black line marks our adopted model for natal BH spin (see eq. 4). Note that the relation between CO core mass and BH mass is non-trivial, as BH mass depends on CO core mass and star mass at the time of core collapse (see Appendix D). These two parameters are influenced by stellar winds (metallicity) and binary component interactions (accretion and mass loss in RLOF/CE).

gular momentum from the core than models that would induce solid body rotation as those that include the Tayler-Spruit dynamo (Spruit 1999, 2002) or stronger angular momentum transport processes (as in MESA; Paxton et al. (2015)). In the convective zones, the transport of angular momentum and chemical species is assumed to be extremely efficient: convective zones are assumed to rotate as a solid body and the chemical composition is homogenized. Our rotating stellar models have an initial equatorial velocity on the ZAMS equal to 40% of the critical velocity (at 100% centrifugal acceleration at the equator balances the gravity). Detailed description of the physics of rotation is given in Eggenberger et al. (2012) and in Ekström et al. (2012).

2.2. Core collapse and BH formation

To determine black hole mass at core collapse of a star, we use the CO core mass formulae (rapid explosions) from Fryer et al. (2012). Since there is a typo in these formulae (published in *The Astrophysical Journal* version) we reintroduce them in the correct form in Appendix D. The progenitor mass at the time of collapse is limited by pulsation pair-instability supernovae and BHs do not form with mass above $\sim 50 M_{\odot}$ (Belczynski et al. 2016a). For our remnant mass prescription, all of the progenitors with zero-age main sequence masses $\sim 20 M_{\odot}$ and above produce BHs.

The stellar models provide the angular momentum in each zone corresponding to a spherical shell in the star. If we assume angular momentum is conserved in the collapse phase, we can calculate the angular momentum of a compact remnant simply by summing the angular momentum of the zones with enclosed mass lower than the compact remnant mass. This can be considered an upper limit to the angular momentum. Angular momentum need not be conserved during the collapse and explosion of a massive star. There are a number of mechanisms that can transfer angular momentum after the bounce of the core (Fryer & Heger 2000; Ott et al. 2006). For fast-spinning cores, secular, dy-

namical and Rossby wave instabilities can develop, reducing the angular momentum in the core. Neutrinos may also carry away angular momentum. These processes can reduce the angular momentum in the proto-neutron star by a factor of a few. If a magnetar develops early in the proto-neutron star, it can remove most of the angular momentum in the core. Note that these angular-momentum loss mechanisms operate effectively in the case of neutron star formation. The angular momentum loss from these mechanisms is minimal if the core collapses quickly to a black hole. We do not include these in our calculations.

The high angular momentum material will not fall directly into the compact remnant but instead first hang up in an accretion disk. This material will lose angular momentum before it accretes onto the black hole. To calculate this angular momentum we limit the maximum angular momentum to the angular momentum at the event horizon under the Newtonian approximation.¹ The assumption lowers somewhat BH spin, assuming angular momentum is lost as the material spirals inward to the event horizon.

From the accreted angular momentum, we calculate the dimensionless BH spin magnitude a_{spin} . Figure 1 shows the BH spins versus CO core mass M_{CO} for our progenitors. Stellar winds during massive star evolution can carry away considerable angular momentum (Georgy et al. 2012; Meynet et al. 2015). For the most massive stars, this mass loss is extensive, removing a lot of angular momentum and producing these slow-spinning BHs. Note that progenitor stars with CO cores less massive than $\sim 20 M_{\odot}$ tend to produce high spin BHs ($a_{\text{spin}} \sim 0.9$), but higher mass stars tend to produce low spin BHs ($a_{\text{spin}} \sim 0$). We approximate the natal BH spin by:

$$\begin{cases} a_{\text{spin}} = 0.9 & M_{\text{CO}} \leq 13 M_{\odot} \\ a_{\text{spin}} = -0.064 M_{\text{CO}} + 1.736 & 13 < M_{\text{CO}} < 27 M_{\odot} \\ a_{\text{spin}} = 0.0 & M_{\text{CO}} \geq 27 M_{\odot}. \end{cases} \quad (4)$$

2.3. Binary evolution

Binary evolution calculations are performed with the upgraded population synthesis code StarTrack (Belczynski et al. 2002, 2008). The existing improvements relevant for massive star evolution include updates to the treatment of CE evolution (Dominik et al. 2012), the compact object masses produced by core collapse/supernovae (Fryer et al. 2012; Belczynski et al. 2012) with the effect of pair-instability pulsation supernovae and pair-instability supernovae (Belczynski et al. 2016a), stellar binary initial conditions set by observations (de Mink & Belczynski 2015), and observationally constrained star formation and metallicity evolution over cosmic time (Madau & Dickinson 2014; Belczynski et al. 2016b). The code adopts by default the fallback-decreased natal kick prescription summarized in Appendix D.

Our principal results are generated via the binary evolution procedures described above, adopting our new BH natal spin prescription. However, the physics of binary evolution remains observationally poorly constrained. To better illuminate the impact of these uncertainties on past and future BH-BH observations, we conducted a limited parameter study, guided by recent developments in CE and RLOF input physics, our access to models with rotation, and the observed properties of GW170104.

¹ We have also investigated a prescription where angular momentum was accreted at the innermost stable circular orbit. This change of prescription has no effect on the slow spin of the heaviest black holes that are the focus of our study, and only modestly increases the rapid BH spins imparted to the lowest-mass black holes.

The fraction of mass retained in the binary (f_a) during stable RLOF is not well established, and could be fully conservative ($f_a = 1$), fully non-conservative ($f_a = 0$), or anywhere in between (e.g., Meurs & van den Heuvel (1989)). Since donor stars are typically the more massive components (at least in a typical BH-BH formation channels) they have a much shorter thermal-timescale than their less massive companions. It means that the large fraction of mass transferred from a massive donor may not be able to accrete onto the companion. So far we have agnostically adopted $f_a = 0.5$, but the recent estimates of thermal timescales in mass transferring BH-BH progenitors resulted (typically) in $f_a < 0.5$ (Stevenson et al. 2017). We now adopt $f_a = 0.2$. This causes the secondary stars (accretors in stable RLOF) to remain less massive than in our previous models and it generates a wider distribution of mass ratios in BH-BH binaries than reported in our earlier calculations.

Even a small amount (\sim few percent of accretor mass) of accretion during RLOF may effectively spin up accreting stars (Packet 1981). With our adopted RLOF retention fraction of $f_a = 0.2$, accretors in BH-BH progenitor binaries typically gain about $10 M_\odot$, which is enough to spin up even very massive stars. This accretion usually happens around the middle (or shortly thereafter) of accretor main sequence life, and therefore it allows for effective rotational mixing and the formation of more massive He and then CO cores. Our Geneva stellar evolution models indicate that the CO core masses in rotating stars (40% critical velocity on the ZAMS; § 2.1) are 20% more massive than in non-rotating models. So far all CO core masses calculated in our binary evolution models were obtained from non-rotating models (Hurley et al. 2000). In our current calculations, we increase CO core mass of accreting low-metallicity ($Z < 0.002$ or $\lesssim 10\% Z_\odot$; $Z_\odot = 0.02$ from Villante et al. (2014)) MS stars by 20%. For high-metallicity stars, effects of rotation on CO core mass are suppressed due to the angular momentum loss through stellar winds (Georgy et al. 2012). All other stars are unaffected by this revision and CO core masses from the non-rotating models are used. This change increases the mass of the second BH, if this BH was not already formed through direct collapse of entire star to a BH (Fryer et al. 2012). It also lowers the spin magnitude of the second BH, if its CO core mass was not very massive ($M_{\text{CO}} < 27 M_\odot$; see eq. 4).

Recent calculations show that the accretion rates onto compact objects in CE inspiral can be reduced even by a factor of 10^{-2} with respect to the rates resulting from the Bondi-Hoyle approximation when the structure of the envelope, in particular the density gradients around the inspiraling object are taken into account (Ricker & Taam 2008; MacLeod & Ramirez-Ruiz 2015a; MacLeod et al. 2017; Murguía-Berthier et al. 2017). MacLeod & Ramirez-Ruiz (2015a) argue that accretion structures forming around compact objects embedded in the CE may span to a large fraction of the envelope radius, and so traverse through substantial density gradients. Introducing gradients in the CE structure enters the angular momentum to the flow around an accreting object (which is not the case in the standard Hoyle formalism) and by doing so, limits the accretion. The steeper the density gradient, the smaller the accretion. The typical values of the density gradients found by these authors introduce a considerable perturbation to the flow. MacLeod & Ramirez-Ruiz (2015b) consider the special case of a CE in a binary system with a NS accretor. In their simulations the NS gains only a few percent of its mass during the inspiral with different simulated envelope structures, in contrast with studies that do not take the structure of the envelope into account, predicting much higher values. Similar results are expected for the CE with BH accretor (Ramirez-Ruiz,

private comm.). The authors stress that due to simplifying assumptions this result is likely an upper limit on the amount of accretion. This conclusion is sustained in the revised study by MacLeod et al. (2017), with improved derivations of drag and accretion coefficients. For most of the density gradients considered by MacLeod et al. (2017) (see their Fig. 6) the accretion rate is well below 10% of Bondi-Hoyle accretion rate. Based on these findings we adopt $f_{\text{bond}} = 5\%$ of Bondi-Hoyle accretion rate onto a BH in CE in our current simulations. This means that now massive BHs ($M_{\text{BH}} \sim 30 M_\odot$) accrete $\sim 0.5 M_\odot$ in a typical CE event, as opposed to $\sim 1.0 M_\odot$ in our earlier calculations ($f_{\text{bond}} = 10\%$).

Compact remnants formed in supernovae can receive proper motions via two classes of engine-driven kicks: asymmetric matter ejecta or asymmetric neutrino emission. For black holes, asymmetric matter ejection mechanisms only work when matter is ejected, as opposed to prompt collapse or complete recapture of all ejected material (“fallback”). In our calculations, we expect that only a small fraction of systems eject a substantial amount of matter, enabling a substantial BH natal recoil kick; see Appendix D. In contrast, asymmetric neutrino emission mechanisms for natal recoil operate even without any mass ejection, and thus could operate in most of the formation channels we expect to be relevant.

Although neutrino mechanisms have been invoked to explain recoil velocities of pulsars and X-ray binaries (Lai & Qian 1998; Repetto & Nelemans 2015), the proposed kick models all require strong magnetic fields (Kusenko & Segrè 1996; Fryer & Kusenko 2006; Socrates et al. 2005) and models without strong magnetic fields are unable to produce significant neutrino kicks (Tamborra et al. 2014).

To understand these neutrino models better, let’s study a few examples. The sterile neutrino oscillation model (Kusenko & Segrè 1996; Fryer & Kusenko 2006) argued that neutrinos produced in the core could oscillate to sterile neutrinos and escape the core. Large magnetic fields align the ions and electrons, forcing both the neutrino scattering and absorption cross sections to be anisotropic. To ensure asymmetric neutrino emission, these strong magnetic fields must be at the surface of last scattering for the neutrinos. If the magnetic field in the core is high enough to align the ions and electrons, the neutrinos in the core will be anisotropic. If these neutrinos oscillate into sterile neutrinos, they can escape, retaining their anisotropies and generating large natal kicks.

Alternatively, the neutrino bubble instability (Socrates et al. 2005) argues that magnetic-acoustic instabilities develop, transporting neutrino radiation to the photosphere. These instabilities carry neutrinos and the luminosity escaping the neutrinosphere will be enhanced at these “bubbles”. If the magnetic-acoustic bubbles are globally asymmetric, the neutrino emission will be as well asymmetric, producing a neutrino-driven kick. Current supernova calculations: (i) do not model the high magnetic fields, (ii) do not sufficiently resolve the hydrodynamics, and (iii) do not include the neutrino oscillation physics to produce these kick mechanisms. So the high BH neutrino driven natal kicks cannot be ruled out.

To mimic asymmetric neutrino emission mechanisms, we explore an alternative phenomenological prescription for BH natal kicks, where we impart kicks random in direction, and with magnitude drawn from a Maxwellian with a given σ , independent of the BH mass or its progenitor history (see Appendix D).

2.4. Calculations

We consider six different realizations (models) of our classical isolated binary evolution. Table 1 gives an overview of the models. In all cases, we assume the stellar spins are initially aligned with the orbital angular momentum of the main sequence binary (but see also Albrecht et al. (2014)). For nascent (initial) BH spin magnitudes we adopt our new physics presented in § 2.2 in all the evolutionary models (old and new). For old models we have redone the calculations with the same input physics but with the addition of the new distribution of natal BH spins. Additionally, we have updated calibration for all models (decrease of rates by factor of 0.926) to account for small inconsistencies in our previous estimates. For example, our adopted IMF with power-law exponent of -2.3 for massive stars (Belczynski et al. 2016b), is inconsistent with the one that was used to derive the SFR that we have adopted from Madau & Dickinson (2014) so our rates need to be corrected (Klencki et al., in prep.).

For each of our models (see Tab. 1) we evolved 2×10^6 binary systems with initial masses of $5 \leq M_1 \leq 150 M_\odot$ (primary) and $3 \leq M_2 \leq 150 M_\odot$ (secondary) at 32 different metallicities spread between $Z = 0.0001$ ($0.005 Z_\odot$) and $Z = 0.03$ ($1.5 Z_\odot$). The numbers of compact binary mergers formed per unit of star forming mass can vary substantially in different models and metallicities, but are generally up to the orders of 10^{-5} , 10^{-6} and $10^{-6} M_\odot^{-1}$ for BH-BH, BH-NS and NS-NS mergers, respectively.

All the compact object mergers are redistributed according to star formation history across cosmic time ($z \approx 0-15$ for Population I and II stars; e.g., Madau & Dickinson (2014)) with account of the delay time between binary formation at Zero Age Main Sequence to the merger. For each merger we use set of gravitational inspiral–merger–ringdown waveforms (IMRPhenomC; Santamaría et al. (2010)) to calculate the signal-to-noise ratio in O1/O2 LIGO detectors. A given merger is considered detectable (depending on its random sky location and orbit orientation in respect to the detectors) if signal-to-noise ratio in a single detector is greater than 8. The full description of the method may be found in Belczynski et al. (2016c,b,a).

Rather than perform a systematic parameter study on spin-orbit misalignment and realignment mechanisms, for each final BH-BH binary we calculate $\chi_{\text{eff,max}}$, the value of χ_{eff} calculated assuming perfect spin-orbit alignment (see eq. 3). For our models M10 and M20 the observationally relevant (heavy) BHs receive little to no natal kick and are weakly misaligned, so we expect $\chi_{\text{eff,max}} \approx \chi_{\text{eff}}$. By contrast, models M13, M23, M25, and M26 adopt some natal BH kicks. In the context of comparing our observations to GW170104 and GW150914 in particular, for these models $\chi_{\text{eff,max}}$ provides a conservative statement about the distribution of χ_{eff} , because spin-orbit misalignment enables χ_{eff} to decrease below the characteristic scale $\chi_{\text{eff,max}}$, becoming even more consistent with the range of χ_{eff} supported by LIGO’s observations, as described below.

3. Results

3.1. Event rates

Table 2 summarizes our predictions for the local (redshift $z \sim 0$) merger rate density, the detection rate in Advanced LIGO’s first (O1) and second (O2) observing runs ($R_{\text{det}} \text{ yr}^{-1}$), and the predicted number of detected events during the full O2 observing run. Over the period November 15, 2016–May 8, 2017 (174 days) LIGO collected 74 days of high-quality doubly-coincident

Table 1. Binary evolution models

Model	Main features
M10	standard input physics: <ul style="list-style-type: none"> – standard BH masses Fryer et al. (2012) – with pair-instability pulsations and SNe – low-to-no BH natal kicks (set by fallback) – 50% non-conservative RLOF – 10% Bondi-Hoyle rate accretion onto BH in CE – no effects of rotation on stellar evolution^a – initial binary parameters Sana et al. (2012) – massive star winds Vink et al. (2001) + LBV^b – BH spin magnitude model adopted (eq. 4)
M13	as in M10, but with: <ul style="list-style-type: none"> – high BH natal kicks ($\sigma = 265 \text{ km s}^{-1}$)
M20	modified input physics, as in M10, but with: <ul style="list-style-type: none"> – 80% non-conservative RLOF (Sec. 2.3) – 5% Bondi-Hoyle rate accretion onto BH in CE – rotation increases CO core mass (by 20%)
M26	as in M20, but with: <ul style="list-style-type: none"> – small BH natal kicks ($\sigma = 70 \text{ km s}^{-1}$)
M25	as in M20, but with: <ul style="list-style-type: none"> – intermediate BH natal kicks ($\sigma = 130 \text{ km s}^{-1}$)
M23	as in M20, but with: <ul style="list-style-type: none"> – high BH natal kicks ($\sigma = 265 \text{ km s}^{-1}$)

Notes.

^a Binary component spins are followed (tides, magnetic braking and change of inertia). However, stellar rotation does not alter internal star properties (He/CO core mass). ^b $(dM/dt)_{\text{LBV}} = 1.5 \times 10^{-4} M_\odot \text{ yr}^{-1}$;

observational data (Abbott et al. 2017a), implying a duty cycle of approximately $F_{\text{duty}} \approx (74/174) \sim 0.425$. O2 is expect to run from Nov 30, 2016 through Aug 25, 2017, for a total of ~ 283 days. Assuming that the LIGO duty cycle remains the same through the observing run, we expect approximately 120 days of coincident data for all of O2 (for comparison Abbott et al. (2016a) reports that there were 51.5 coincident data in entire O1). The predicted number of detections in O2 is obtained from $N_{\text{det}} = (120/365) R_{\text{det}}$. In this prediction the detection distance for NS-NS mergers is about ~ 70 Mpc (defined as the radius of sphere that equals volume contained in peanut-shaped LIGO response function; $z < 0.016$), with corresponding horizon distance of ~ 160 Mpc (for an optimally located and oriented binary; $z < 0.036$). For comparison, the maximum (horizon) redshift to which our most massive BH-BH mergers are detected is $z \lesssim 0.63$.

Two major observations can be made:

1. Assuming high natal kicks for both NSs and BHs ($\sigma_{\text{ID}} = 265 \text{ km s}^{-1}$, models M13 and M23) greatly reduces the predicted number of BH-BH and BH-NS mergers (by factors of ~ 30 and ~ 10 , respectively) with respect to models with kick velocities lowered by fallback (M10 and M20), while only slightly affecting the NS-NS systems (less than a factor of 2).
2. The inclusion of updated physical assumptions for mass transfer in model M20 with respect to M10 (see Tab. 1 for details) increases the merger rates of all types of systems, generally by a factor no larger than 2 (with the exception of the BH-NS merger density, which increases by a factor of ~ 4).

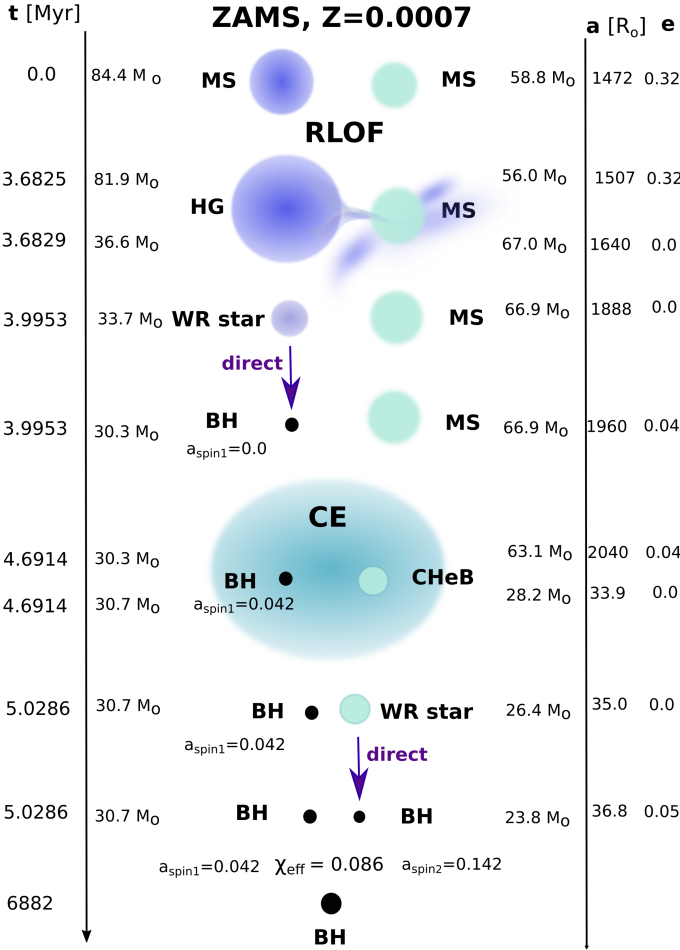


Fig. 2. Example of the formation of a BH-BH merger similar to GW170104: parameters of the merger are within the 90% credible levels reported by LIGO. This example follows from the classical isolated binary evolution channel and was obtained with the upgraded StarTrack population synthesis code. In this model (M20) massive BHs do not receive natal kicks and their spins are aligned with binary angular momentum ($\Theta_1 = \Theta_2 = 0$ deg) producing an upper limit on the effective spin parameter (χ_{eff}). For details of this evolutionary sequence see Appendix A.

The predicted BH-BH merger rate densities vary between 6 and 345 $\text{Gpc}^{-3} \text{yr}^{-1}$ across our models, and are able to account for the entire allowable range determined by existing LIGO detections (12–213 $\text{Gpc}^{-3} \text{yr}^{-1}$ Abbott et al. (2017b)). In particular, our models with BH natal kicks decreased by fallback (small kicks for low mass BHs and no kicks for massive BHs) yield the highest merger rate densities: $\sim 200\text{--}350 \text{Gpc}^{-3} \text{yr}^{-1}$, implying $\sim 30\text{--}60$ BH-BH detections during the entire O2 observing run (models M10 and M20). The models with high (unattenuated by fallback) BH natal kicks predict the smallest rates $\sim 10 \text{Gpc}^{-3} \text{yr}^{-1}$ ($\sim 1\text{--}2$ detections in O2: models M13 and M23). Naturally, models with small-to-intermediate (unattenuated) natal kicks generate moderate BH-BH merger rate densities: $\sim 100 \text{Gpc}^{-3} \text{yr}^{-1}$ for M26 (~ 10 detections in O2) and $\sim 50 \text{Gpc}^{-3} \text{yr}^{-1}$ for M25 (~ 5 detections in O2).

In Table 2 we also include predicted detection rates of BH-BH mergers similar to GW170104, which we choose to identify as those systems with a total mass within the LIGO 90% credible interval: $45.7 < M_{\text{tot}} < 56.6 M_{\odot}$. We find that all our models produce BH-BH mergers resembling GW170104 in terms

Table 2. Local merger rates and LIGO O1/O2 detection rates

Model Merger type	Rate density ^a [$\text{Gpc}^{-3} \text{yr}^{-1}$]	O1/O2 rate ^b [yr^{-1}]	O2 ^c [120 days]
M10			
NS-NS	68.2	0.088	0.03
BH-NS	25.8	0.416	0.14
BH-BH	205	111.6	36.7
1:GW17 ^d		17.97	5.91
M13			
NS-NS	50.8	0.068	0.02
BH-NS	2.01	0.029	0.01
BH-BH	6.19	3.187	1.05
1:GW17 ^d		0.236	0.08
M20			
NS-NS	88.3	0.111	0.04
BH-NS	107	1.588	0.52
BH-BH	345	170.7	56.2
1:GW17 ^d		27.71	9.12
M26			
NS-NS	115	0.146	0.05
BH-NS	41.7	0.591	0.19
BH-BH	97.2	41.28	13.6
1:GW17 ^d		6.065	2.00
M25			
NS-NS	108	0.140	0.05
BH-NS	16.4	0.242	0.08
BH-BH	45.1	22.45	7.39
1:GW17 ^d		3.818	1.26
M23			
NS-NS	55.2	0.070	0.02
BH-NS	3.42	0.049	0.02
BH-BH	11.8	5.342	1.76
1:GW17 ^d		0.529	0.17

Notes.

^a Local merger rate density at redshift $z = 0.0$.

^b Detection rate for LIGO O1 and O2 observational run.

^c Number of detections expected in O2.

^d BH-BH mergers resembling GW170104, with: $45.7 < M_{\text{tot}} < 56.6 M_{\odot}$

of total mass. Typically, such systems contribute $\sim 10\%$ of the entire BH-BH detection rate (e.g., these are 16% of the mergers in M20). An example of the evolution of a progenitor of a GW170104-like BH-BH merger is shown in Figure 2 (see Appendix A for a detailed description of this evolutionary pathway).

3.2. Reproducing the parameters of observed BH-BH binaries

Figure 3 shows the detector-frame distributions of primary BH masses (i.e., the more massive BH, M_{BH1}) and mass ratios ($q = M_{\text{BH2}}/M_{\text{BH1}}$) of BH-BH mergers in models with BH natal kicks decreased by fallback (M10 and M20). We show the entire population of events detectable with the O1/O2 LIGO, as well as restricting to systems in which the total mass falls within the 90% credible limits for GW170104.

The primary BH mass is relatively insensitive to the input physics updates presented in § 2.3, which is why the M_{BH1} distribution does not change significantly between model M10 and M20. The distributions span the range from ~ 5 up to

$\sim 50 M_{\odot}$, with the upper limit imposed by the occurrence of pair-instability pulsation supernovae in stars with He core mass $45 \lesssim M_{\text{He}} \lesssim 65 M_{\odot}$ (Heger & Woosley 2002; Woosley & Heger 2015). It is assumed that the pair-instability pulsation supernovae remove star layers above inner $45 M_{\odot}$ just prior to core collapse, limiting the remnant BH mass (Belczynski et al. 2016a). This assumption is responsible for the peak just above $40 M_{\odot}$, although future pair-instability simulations may show that this peak is much broader than we have assumed. Nevertheless, our simulations recover the entire 90% credible limit for M_{BH1} in GW170104.

In the case of model M10 the mass ratio distribution is clearly skewed towards systems with similar component masses ($q \gtrsim 0.7$). Model M20, on the other hand, produces additional BH-BH mergers with moderate mass ratios down to $q \approx 0.3$ and covers the entire range of mass ratio constraint for GW170104. The introduction of 80% non-conservative RLOF in model M20, as contrasted with 50% RLOF mass loss in model M10, is the major cause of this difference (see § 2.3 for details).

Figure 4 shows the detector-frame distributions of parameters of BH-BH mergers in models with with kicks decreased by fallback (M10 and M20) and small, but unattenuated (model M26) BH natal kicks: the total redshifted mass (z is a merger redshift):

$$M_{\text{tot},z} = (M_{\text{BH1}} + M_{\text{BH2}})(1 + z) \quad (5)$$

versus mass ratio q , as well as the maximum effective spin parameter $\chi_{\text{eff,max}}$ versus mass ratio q . For context, we also superimpose the approximate 90% confidence intervals reported for the four LIGO events. In the right panels, GW170104 and GW150914 have χ_{eff} distributions that seem only modestly consistent with our predictions in which we adopted the conservative assumption of no spin-orbit misalignment (i.e., $\chi_{\text{eff,max}} = \chi_{\text{eff}}$). However, we emphasize the comparisons illustrated in the right panels of this figure are doubly conservative. On the one hand, spin-orbit misalignment in our models with significant BH natal kicks further decreases χ_{eff} below $\chi_{\text{eff,max}}$ (Gerosa et al. 2017, in prep.). On the other hand, as noted in Appendix B, the reported LIGO constraints on χ_{eff} were estimated by adopting some specific prior assumptions. The assumptions used – that BH spins are equally likely to point in any direction, relative to the orbit – are consistent with dynamical capture but inconsistent with our formation scenarios. In Appendix B we illustrate by example how the most constraining upper limit on χ_{eff} (< 0.09 for GW170104; Abbott et al. (2017b)) might change to a much less restrictive limit ($\chi_{\text{eff}} < 0.2$) by adopting a more suitable prior for that quantity.

We see that all the LIGO BH-BH mergers observed thus far are reproducible in our simulations and are therefore consistent with formation from isolated binaries. In model M10 massive BH-BH mergers ($M_{\text{tot},z} \gtrsim 40 M_{\odot}$) are systems with high mass ratios ($q \gtrsim 0.7$, see also bottom panel of Fig. 3). In model M20 we find that the mass ratio distribution can change substantially for different assumptions concerning mass transfer: models M20, M23, M25, M26, with more non-conservative mass transfer than assumed in model M10, allow for the formation of massive mergers with mass ratios as low as $q \approx 0.3$. In these models the formation of systems with masses and mass ratios measured for GW170104 is not only possible but also typical.

Note that the shape of the distributions in Figure 4 is very similar for models M20 and M26 – the variations of BH natal kick velocities have major impact on the merger rates (see Tab. 2) but only minor impact on the binary properties.

Figure 5 (left panel) shows the total redshifted mass distribution of compact binary mergers detectable with the O1/O2 LIGO. We also show the O2 sensitivity (assuming 120 effective days of coincident data collection). All of the reported LIGO observations (marked) fall within the most probable range of redshifted masses we predict from our simulations ($20 \lesssim M_{\text{tot},z} \lesssim 100 M_{\odot}$). It is found that the shape of the redshifted total mass distributions for models M10, M13 M25, and M26 (not shown) are very similar to those in models M20 and M23 (shown in Fig. 5). The only significant difference between the distributions is in the overall merger rate density; these are shown in the right panel for all models. In the right panel we compare the local ($z = 0$) intrinsic merger rate densities of BH-BH mergers for all our models (see also Tab. 2) with the current limits imposed by the four LIGO detections ($12\text{--}213 \text{ Gpc}^{-3} \text{ yr}^{-1}$; shown by the blue double-headed arrow).

3.3. The black hole spin distribution and the role of accretion

In our BH natal spin prescription, BH are typically born with high or low spin, but this spin can be modified by accretion from a binary component. Even though the amount of matter accreted in our calculations is very modest, the accretion-induced spinup of some of the first-born, heavy black holes is sufficient to impart spins that begin to be observationally relevant, in comparison with constraints on χ_{eff} (e.g., for GW170104). To quantify the extent to which different assumptions can adjust accretion-induced spinup, we use models M10 and M20, which adopt different mass transfer and accretion prescriptions.

Figure 6 shows the detector-frame distributions of the amount of mass accreted by the primary BHs in our BH-BH mergers for the M10 and M20 models (M_{acc} , top panel), which in turn are related to the distributions of the individual BH spins (middle and bottom panels). The second two panels show the effect of this accretion on the corresponding spin distributions, focusing on the part of the distribution associated with low BH spins ($a_{\text{spin}} < 0.3$) and the other on large BH spins ($a_{\text{spin}} > 0.7$). We find that the majority of our BHs fall into either one of those two extremes, which results from the combination of adopted natal BH spins (eq. 4) and the BH mass distribution (Fig. 4). In the majority of cases the primary BH accretes only during a CE phase, and the amount of mass accreted is very low ($M_{\text{acc}} \lesssim 1.0 M_{\odot}$ in M10 and $M_{\text{acc}} \lesssim 0.5 M_{\odot}$ in M20) compared to the primary BH mass (see top panel of Fig. 3). For that reason the increase of spin magnitude for massive BHs is relatively small. These massive BHs start with very low initial spins ($a_{\text{spin,init}} \approx 0$) and end up with final spins of the order of $a_{\text{spin,final}} \approx 0.15$ for model M10 and $a_{\text{spin,final}} \approx 0.05$ for model M20. However, it is important to note that even if in fact all massive BHs have negligible spins at birth, they can gain measurable spin from binary accretion ($a_{\text{spin,final}} \approx 0.1$). By contrast, for rapidly rotating (low mass) BHs, this accretion has little relative impact on the BH's spin magnitude.

4. Discussion

4.1. LIGO observations versus models

Three of the four binary black hole mergers detected by LIGO contain black holes with component masses $> 20 M_{\odot}$ (Abbott et al. 2016d,c,a; Abbott et al. 2017b). These heavy black holes are naturally explained via formation in a low-metallicity environment, consistent with prior predictions (Belczynski et al. 2010b). The low observed χ_{eff} of these mergers is inconsistent

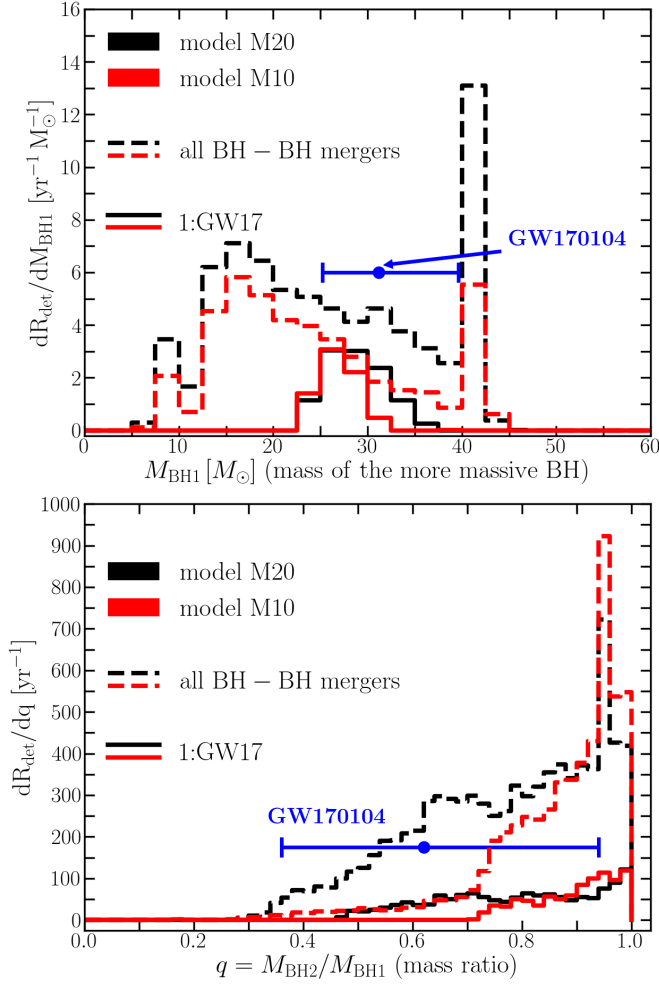


Fig. 3. Properties of BH-BH mergers models M10 and M20. We show the entire population of BH-BH mergers detectable with the O1/O2 LIGO (dashed lines), as well as the subpopulation of mergers resembling GW170104 in terms of their total mass (solid lines). The horizontal position of GW170104 (with 90% credible levels) is marked (vertical position has no meaning). Primary BH mass (top panel) and mass ratio (bottom panel) of GW170104 are recovered by our classical isolated binary evolution channel.

with BH spins with large components along the direction of the orbital angular momentum. LIGO’s observations already provide an opportunity to assess the viability of different formation models.

The absence of any evidence for significant aligned spins disfavors isolated binary homogeneous evolution models which explicitly predicted significant and aligned BH spins (e.g. de Mink & Mandel 2016; Marchant et al. 2016). Another class of models that stems from classical isolated binary evolution predicts that the BH-BH mergers with short delay times will have rapidly spinning secondary BHs, while for longer delay times the BH spins may be small (Kushnir et al. 2016; Zaldarriaga et al. 2017; Hotokezaka & Piran 2017). These arguments are based on a tidal spin-up of a Wolf-Rayet (WR) star before it collapses to form the second BH. Convective cores of WR stars are rather small ($\lesssim 1 R_{\odot}$; Kushnir et al. (2016)), while the typical BH-WR star binary orbits in our models are much larger (\sim tens of R_{\odot} ; see Fig. 2, see also Fig. 1 of Belczynski et al. (2016b)) and thus the tidal forces working on the convective cores are not expected to be very effective. We find that only a small fraction of our pro-

genitors consist of WR stars of size comparable to their Roche lobe. It is only in these systems that, potentially, tidal forces might result in the formation of a rapidly spinning secondary BH even if this is a heavy BH. We note that current GW observations provide essentially no constraints on the spin of the secondary BHs; e.g., see the right hemispheres of Fig. 5 of Abbott et al. (2016a).

Alternatively, the two heavy binary black holes and one heavy candidate detected so far are consistent with many other formation scenarios. In particular, two major scenarios are considered: classical isolated binary evolution (Tutukov & Yungelson 1993; Lipunov et al. 1997; Nelemans et al. 2001; Belczynski et al. 2002; Voss & Tauris 2003; Dominik et al. 2012; Mennekens & Vanbeveren 2014; Belczynski et al. 2016b; Eldridge & Stanway 2016; Stevenson et al. 2017) and dynamical formation channel (Portegies Zwart et al. 2004; O’Leary et al. 2007; Sadowski et al. 2008; Downing et al. 2010; Benacquista & Downing 2013; Bae et al. 2014; Mapelli 2016; Hurley et al. 2016; Rodriguez et al. 2016b; Askar et al. 2017). These two scenarios predict very different distributions of spin-orbit misalignment, with dynamical capture generating uniform distribution of misalignments (with both small and large BH tilt angles equally favored).

GW170104 is the only observation that potentially supports a large degree of spin-orbit misalignment, with an effective spin parameter of $\chi_{\text{eff}} = -0.12^{+0.21}_{-0.30}$, with 90% credible intervals (Abbott et al. 2017b). However, the individual BH spin magnitudes and spin misalignment angles required to demonstrate misalignment have not been well measured (Abbott et al. 2017b). As a result, two different types of BH-BH binary can be reconciled with this observation²:

1. If GW170104 spin magnitudes are small for both BHs ($a_{\text{spin1}} \lesssim 0.1$, and $a_{\text{spin2}} \lesssim 0.1$) then both BH spin tilts are not constrained (e.g., they can be fully aligned: $\Theta_1 \approx 0$ deg and $\Theta_2 \approx 0$ deg) to generate a gravitational waveform consistent with the measured effective spin parameter: $-0.42 < \chi_{\text{eff}} < 0.09$.
2. If the spin magnitudes of both components of GW170104 are high ($a_{\text{spin1}} \gtrsim 0.9$ and $a_{\text{spin2}} \gtrsim 0.9$), then:
 - (i) then for highly misaligned more massive BH spin ($\Theta_1 \gtrsim 150$ deg) the less massive BH spin can only be moderately tilted ($0 < \Theta_2 < 90$ deg), and
 - (ii) if tilts of both BHs are the same they must be significant, but not too large ($84 \lesssim \Theta_1 = \Theta_2 \lesssim 118$ deg) to match LIGO estimate: $-0.42 < \chi_{\text{eff}} < 0.09$.

If the first case is true, then the measured effective spin parameter can not be used to distinguish between classical isolated binary and dynamical formation scenarios. We have demonstrated that it is possible, within classical isolated binary model uncertainties, to form BH-BH binaries with low spinning BHs and with other physical parameters resembling GW170104 (see Fig. 2 and § 3) and LIGO have reported that spin magnitudes of merging BHs in GW170104 may be small and that even zero spins can not be excluded (Abbott et al. 2017b). This means that both formation scenarios are able to generate small values of χ_{eff} that are consistent with the LIGO measurement.

If the second case is true, then this may seem indicative that GW170104 has formed by dynamical capture either in globular cluster or dense nuclear cluster. Dynamical capture favors

² To obtain the following requirements on tilts we have varied GW170104 mass ratio within 90% LIGO credible limits: $q = 0.34\text{--}0.93$ (Abbott et al. 2017b) along with eq. 1 rewritten as $\chi_{\text{eff}} = (a_{\text{spin1}} \cos \Theta_1 + qa_{\text{spin2}} \cos \Theta_2)/(q + 1)$

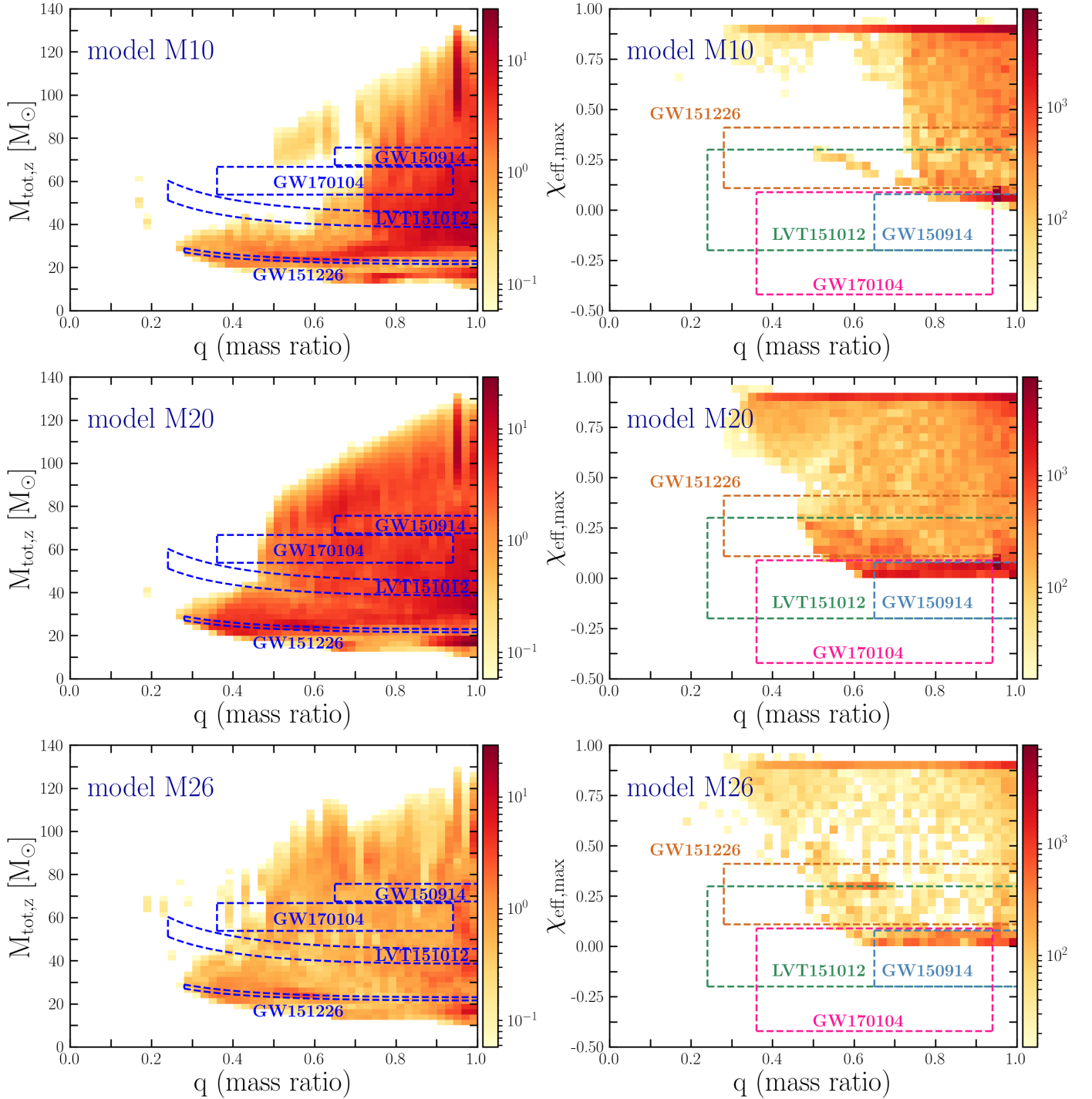


Fig. 4. Left: Detector-frame distributions of BH-BH binary redshifted masses, $M_{\text{tot},z}$, and mass ratios, q . Top panels: model M10 (previous calculations), middle panels: model M20 (new, less conservative mass transfer), and bottom panels: model M26 (M20 with $\sigma_{\text{ID}} = 70 \text{ km s}^{-1}$ BH natal kicks). Right: Detector-frame distributions of BH-BH binary maximum effective spins, $\chi_{\text{eff,max}}$ (see Eq. 3), and mass ratios, q . We also show the approximate 90% confidence intervals reported for the four LIGO events. Even though we are double conservative (by comparing upper limits on effective spins and by assuming unfavorable priors on observed χ_{eff} , see Appendix B) our classical isolated binary evolution models are consistent with all the four LIGO detections. Note the color log-scale and the peak of events (red) with small maximum effective spins ($\chi_{\text{eff,max}} \lesssim 0.1$). All the plots are made in the detector frame, showing BH-BH mergers detectable with LIGO O1/O2 sensitivity. The quantities marked with colors are: $dR_{\text{det}}/dM_{\text{tot},z}dq$ ($\text{yr}^{-1} \text{M}_{\odot}^{-1}$, left panels), and $dR_{\text{det}}/d\chi_{\text{eff}}dq$ (yr^{-1} , right panels).

random BH spin tilts so there is 50% chance of each BH spin to be misaligned by more than 90 deg. However, high BH natal kicks can significantly misalign at least firstly-formed BHs to high tilt angles. In case of the first BH formation, orbits are typically wide and it is easy to significantly change orbit orienta-

tion (Kalogera 2000; O’Shaughnessy et al. 2017) with respect to BH spin and then precession can increase misalignment (Gerosa et al. 2013). On the other hand, CE evolution and tidal interactions between the first and the second BH formation (see Belczynski et al. (2016b) for evolutionary sequences) can re-align

the first BH spin with binary angular momentum. Whether high BH natal kicks for massive BHs are possible, or whether such events are frequent enough to produce detectable events is not at all clear at the moment. Moreover, other processes can also potentially lead to the misaligned spins of star in binaries (Albrecht et al. 2014).

These two physically separate formation mechanisms might leave their distinctive (statistical) imprint on the whole population's spin distribution, notably the distribution of χ_{eff} (Farr et al. 2017), which is conserved on astrophysical timescales (Racine 2008; Gerosa et al. 2015). However, the population of binary black hole mergers observed to date does not provide enough information to distinguish between these two channels. We defer systematic discussion of black hole spin misalignment, Bayesian model selection, and the strength of BH natal kicks to a different paper (Gerosa et al. 2017, in prep.).

4.2. Black holes in globular clusters

If we were to assume that the effective spin (χ_{eff}) measurement of GW170104 was the evidence of a dynamical formation channel, but that the other three binaries were formed in isolation, then observed rate is in tension with the predictions for the merger rate from globular clusters. The BH-BH merger rates in the dynamical channel are much smaller than in the classical isolated binary evolution channel (see Appendix C in comparison to Figure 5).

Furthermore, no black holes have been observed in globular clusters. Although several radio-selected systems were suggested to be globular-cluster black holes (Strader et al. 2012; Chomiuk et al. 2013; Tetarenko et al. 2016; Bahramian et al. 2017), none of these candidates have been yet confirmed by further observations. The LMXB X9 in 47 Tuc, selected through its unusual X-ray to radio luminosity ratio, exhibits both short (28 min) and long (6.8 day) periodicities which have been interpreted by Bahramian et al. (2017) as orbital and super-orbital periods respectively suggesting that X9 is the first known ultra-compact black-hole X-ray binary. However, Charles & Lasota (2017, in prep.) put forward an alternative interpretation where the short period is the spin period of a magnetic white dwarf in a ~ 2 hr orbit, i.e. that it is instead an Intermediate Polar. According to this interpretation the long period is due to a tilted/warped disc (Murray et al. 2002), a result of interactions with the donor's magnetic field. This model naturally accounts for the observed large X-ray modulation with little variations at other wavelengths, a feature difficult to explain in a black hole scenario.

Additionally, there are about ~ 20 BHs known in the Galactic field and a few more in near-by galaxies (Casares & Jonker (2014), Corral-Santana et al. (2016); all observed in isolation). It may seem possible that these systems have formed in globular or nuclear clusters and were ejected into galactic fields. However, in case of the Galactic BH systems their spatial distribution seems to be consistent with the formation in the Galactic disk (field population) and not in halo where globular clusters reside (Belczynski et al. 2016c; Mandel 2016; Repetto et al. 2017). Further support of non globular cluster origin may arise from some reported super-solar metallicities of donor stars in Galactic BH X-ray binaries (V404 Cyg González Hernández et al. (2011); V4641 Sgr Orosz et al. (2001); XTE J1118+480 González Hernández et al. (2006); GRO J1655-40 Israelian et al. (1999), González Hernández et al. (2008); A0620-00 González Hernández et al. (2004)).

4.3. Comparison with Postnov & Kuranov (2017)

Postnov & Kuranov (2017) have recently reported that chirp masses and effective spin parameters of GW150914, LVT151012 and GW151226 are “difficult to reproduce simultaneously” with their classical isolated binary evolution model. This stands in clear contradiction with our results (e.g., see Fig. 4 and Fig. 5). However, their study suffers from two major classes of problems which leads us to question their conclusions: their stellar and binary physics; and their neglect of any discussion of the frequency with which low-metallicity gas can form stars and massive BHs.

The first class of problems is connected with the input physics of Postnov & Kuranov (2017) model of classical isolated binary evolution. (a) Their model does not form heavy binary black holes, except at zero metallicity (i.e., Population III stars). In particular and in tension with most other recent investigations of low-metallicity BH formation, they do not form heavy BH-BH binaries (here, a chirp mass $> 12 M_{\odot}$) even for $Z = 10^{-4} = 0.005 Z_{\odot}$, let alone at any higher metallicity; see their Fig.1 and 2. By contrast, most studies of single and binary stars at low metallicity invoke low mass loss and produce many heavy BHs, with individual masses up to $100 M_{\odot}$ (Zampieri & Roberts 2009; Mapelli et al. 2009; Belczynski et al. 2010a; Spera et al. 2015; Abbott et al. 2016b). Despite the fact that pulsation pair-instability supernovae may bring the maximum BH mass down to $\sim 50 M_{\odot}$, chirp masses as high as $\sim 50 M_{\odot}$ are still expected in the classical isolated binary evolution (Belczynski et al. 2016a). (b) The evolutionary sequences that are reported (their Tab.1) allow for Hertzsprung gap stars to initiate CE. The authors adopted this approach without addressing physical arguments indicating that massive donors with radiative envelopes (e.g., HG stars) are not likely to initiate a CE phase, but rather evolve through fast thermal-timescale mass transfer (Pavlovskii et al. 2017). (c) Common envelope evolution calculations rely on an accurate calculation of the envelope binding energy. The authors adopt an approximation whereby the binding energy of the envelope is assumed to be a constant (and unknown) fraction of a simple, structure-independent estimate of the binding energy of the envelope (λ ; Dewi & Tauris (2000)). This constant approximation explicitly omits the known, strong dependence of this parameter on the mass, radius, and metallicity of the donor star (Tauris & Dewi 2001; Podsiadlowski et al. 2003; Xu & Li 2010; Loveridge et al. 2011; Kruckow et al. 2016). This dependence has been incorporated into several recent calculations of compact binary formation. These three pieces of input physics are crucial ingredients in any reliable formation scenario for BH-BH binaries in the framework of classical isolated binary evolution.

(d) The second problem is that the Postnov & Kuranov (2017) study does not produce a prediction about the frequency of mergers at low redshift that can be compared to observations. The authors perform population synthesis on several independent batches of star-forming gas with different metallicities, without accounting for how likely these conditions are to occur in our universe over cosmic time. They have not folded in the cosmological star formation history and the metallicity evolution (and distribution) of past star formation, in contrast to this study or other studies (Dominik et al. 2015; Belczynski et al. 2016a). In particular, their formation scenario for massive BH binaries like GW150914 and GW17104 must invoke Population III stars, which both constitute a small fraction of all past star formation and which formed long ago. Both the rarity and age of Population III star formation will dramatically diminish the potential impact of this scenario on the low redshift BH-BH merger rate.

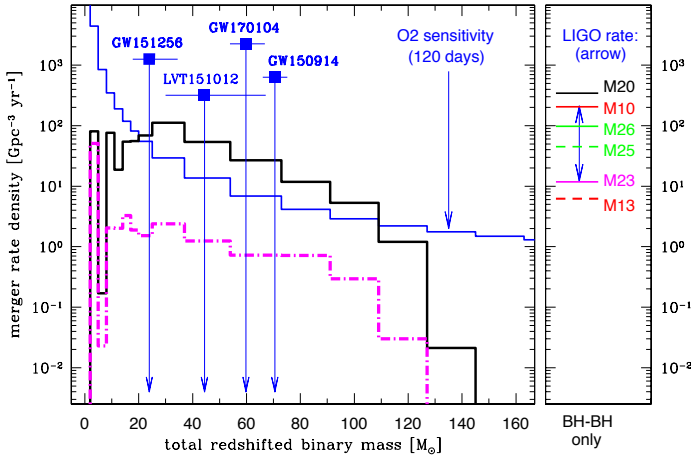


Fig. 5. *Left:* Redshifted total merger mass distribution for models M20 and M23. The O2 LIGO sensitivity is marked; the most likely detections are expected when models are closest to the sensitivity curve. We also mark LIGO BH-BH merger detections (vertical positions have no meaning), all of which fall within the most likely detection region: $M_{\text{tot},z} \sim 20\text{--}100 M_{\odot}$. *Right:* Source frame BH-BH merger-rate density of our models for the local Universe ($z = 0$). The current LIGO O1/O2 BH-BH merger rate is $12\text{--}213 \text{ Gpc}^{-3} \text{ yr}^{-1}$ (blue double-headed arrow). Note that our models with fallback-attenuated BH natal kicks (M10, M20) are at the LIGO upper limit, while our models with full BH natal kicks are at the LIGO lower limit (M13, M23). Models with small (M26) and intermediate (M25) BH kicks fall near the middle of the LIGO estimate.

Other studies which combine binary evolution with time- and metallicity-dependent star formation suggest that Population III stars are unlikely to be responsible for the observed events (Belczynski et al. 2016d), despite some earlier contradictory claims (Kinugawa et al. 2014, 2016).

(e) On a closely related note, Postnov & Kuranov (2017) do not account for LIGO’s highly mass-dependent sensitivity. For example, they do not account for the fact that LIGO’s substantial reach to the heaviest BHs even now extends to redshifts of ~ 0.5 , where the star formation rate is noticeably higher (and at lower average metallicity) than the present-day star formation.

In short, the authors adopted stellar and binary physics which cannot produce massive binary black holes and thus several of LIGO’s observations except through rare Population III formation channel. They do not assess whether their scenario can produce the observed rates and physical properties of LIGO events.

5. Conclusions

Previous work to model the population of BH-BH mergers produced by classical isolated binary evolution naturally predicts the formation of heavy black holes in low-metallicity environment, with rates matching the current LIGO observations (Belczynski et al. 2010b; Dominik et al. 2015). Previous work on these scenarios has not carefully explored the distribution of expected spin magnitudes and orientations. Our goal here is not to prove that classical isolated binary evolution is the only possible explanation for the observed LIGO events, but rather to investigate whether this scenario is compatible with current mass, merger rate and spin measurements. The observations already disfavor models which predicted significant, aligned spins for massive BH binaries (see e.g. de Mink & Mandel 2016; Marchant et al. 2016). However, as pointed out by Farr et al. (2017), the small observed values of χ_{eff} for GW150914 and

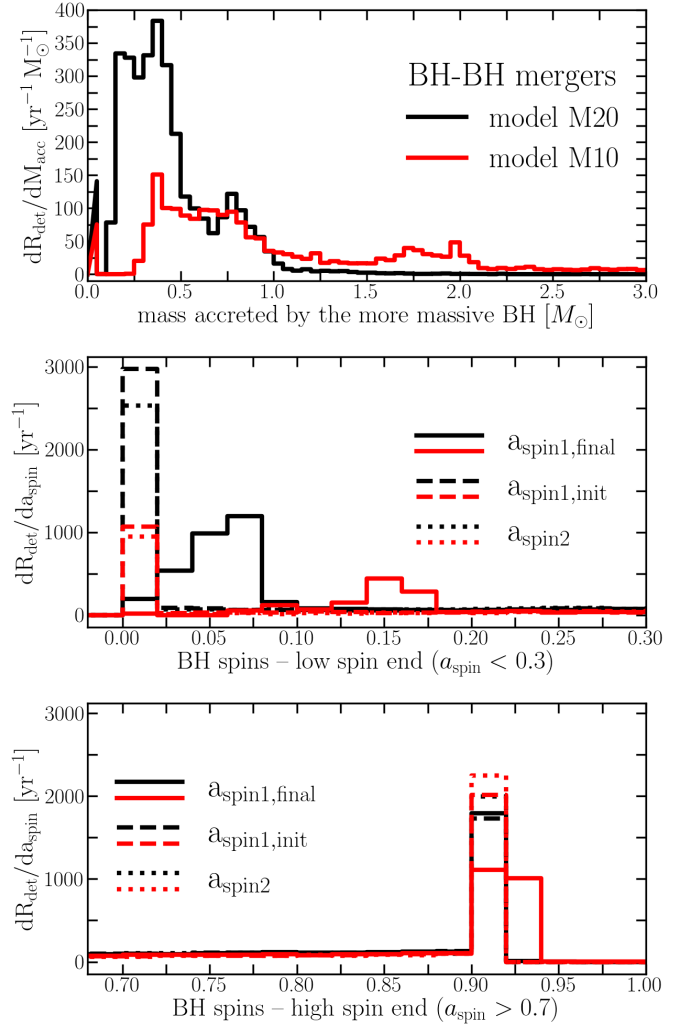


Fig. 6. Comparison of individual BH spins between models M10 and M20. Top panel: Distribution of the amount of mass accreted by the more massive BH during the binary evolution. In the majority of cases the primary BH accretes only during a CE phase, in which case we adopt either a 5% (model M20) or 10% (model M10) of the Bondi-Hoyle accretion rate. This difference between our models is clearly visible in the plot. Middle and bottom panels: Distributions of individual BH spins of detectable BH-BH mergers in our simulations. For better readability we split the distributions into two separate plots for low ($a_{\text{spin}} < 0.3$) and high spins ($a_{\text{spin}} > 0.7$), as the majority of our BHs fall within either one of those extremes; in the range not shown ($0.3 < a_{\text{spin}} < 0.7$) all the distributions remain low and constant. We show initial (dashed lines) and final (solid lines) spins of the primary BHs, which are increased due to mass accretion during mass transfer. Note that the amount of accreted mass is typically very small ($\lesssim 1.0 M_{\odot}$) compared to the primary BH mass (see Fig. 3), which is why the increase from initial to final spins is rather low (from $a_{\text{spin}} = 0$ to ~ 0.05 in M20 and to ~ 0.15 in M10). Spins of the secondary BHs (dotted lines) are also shown.

GW170104 are consistent with either (i) nonzero spins and large BH spins tilts, or (ii) moderate or small spin magnitudes.

We have introduced a physical model that incorporates detailed stellar evolution of rotating progenitor stars through core collapse to predict the natal black hole spin, and simulations with accretion and spin-up during binary evolution to deduce the “final” spin of the black holes in a binary. Our model suggests that while low-mass BHs can be rapidly rotating, massive BHs such as those observed by LIGO will be born with small natal spins,

which are at best modestly increased by binary accretion over their lifetime. However, note that by no means we can (nor claim to) exclude high natal spins for heavy BHs of stellar origin. As discussed in § 2.1 and § 2.2, there are various stellar rotation models and some could generate alternative BH spin distributions than what we have estimated in our analysis.

Our main conclusion is that the current LIGO observations of these heavy black holes' spins do not favor dynamical BH-BH formation scenario over classical isolated binary BH-BH formation scenario. This is consistent with the analysis of Farr et al. (2017), who argued (using an ad-hoc model for black hole natal spins) that LIGO's observations of "heavy" black holes required either small BH spins, or strong misalignment. Our work shows that heavy black holes with small spins are a perfectly viable possibility in the context of isolated binary evolution.

More specifically, we explored how several different physical assumptions affect the likelihood of producing binary black hole mergers with rates, masses and spins compatible with GW170104. We demonstrated conclusively that the formation of GW170104 occurs naturally in several classical isolated binary evolution models.

If the spin magnitudes of the BHs in GW170104 were not small, then the most natural explanation would be formation through dynamical capture, which can produce strongly misaligned spins. However, LIGO measurements of the BH spin magnitudes in GW170104 are inconclusive (Abbott et al. 2017b). Unfortunately, the spin magnitudes of massive BHs with $M_{\text{BH}} > 20 M_{\odot}$ are not constrained by other observational means. Indeed, the three most massive BHs in wind-fed high mass X-ray binaries (which are potential double compact object progenitors) do not reach such high masses³, but we list them here for completeness: LMC X-1 $M_{\text{BH}} = 10.9 \pm 1.6 M_{\odot}$ ($a_{\text{spin}} = 0.92$; Gou et al. (2009)), Cyg X-1 $M_{\text{BH}} = 14.8 \pm 0.1 M_{\odot}$ ($a_{\text{spin}} > 0.983$; Gou et al. (2014)), M33 X-7 $M_{\text{BH}} = 15.7 \pm 1.5 M_{\odot}$ ($a_{\text{spin}} = 0.84$; Liu et al. (2010)). Note that high spins of these BHs are fully consistent with our natal BH spin model (see Fig. 1).

It is possible that future LIGO detections will provide evidence for dynamical formation of BH-BH mergers. Previous studies imply that a smoking-gun of this scenario would be the observation of BH-BH mergers with highly anti-aligned spins ($\Theta_i > 90^\circ$) resulting from random dynamical capture, and/or one of the two binary components in the mass range $55 \lesssim M_{\text{BH}} \lesssim 135 M_{\odot}$. The lower limit corresponds to pair-instability pulsation supernova effects on the presupernova star and on the remnant BH mass (Heger & Woosley 2002; Woosley 2017), while the upper limit corresponds to the end of the pair-instability supernova process, that is believed to disrupt the entire star without BH formation (Fryer et al. 2001; Heger & Woosley 2002). The lack of BHs in this mass range is referred to as the "second mass gap" (Belczynski et al. 2014; Spera et al. 2015; Marchant et al. 2016). It seems unlikely that isolated binaries can fill this gap, but repeated BH-BH mergers in dense environments could produce such heavy BHs, and then we would expect them to have moderate spins $a_{\text{spin}} \approx 0.7$ (Gerosa & Berti 2017; Fishbach et al. 2017). Alternatively, if a BH with mass within the second mass gap is detected with a low spin, it may point to (i) either some inconsistencies in pair-instability supernova theory, or to (ii) the primordial origin of such a BH (Sasaki et al. 2016; Eroshenko 2016; Green 2017).

If LIGO observations of heavy BH binaries continue to be consistent with $\chi_{\text{eff}} \approx 0$, this would (statistically) suggest that

low BH natal spins are common for heavy BHs. In this case, our work suggests that measurements of χ_{eff} alone are insufficient to distinguish between the dynamical formation channel and classical isolated binary evolution channel. Conversely, an classical isolated binary origin would be more difficult to reconcile with future discoveries of *several* binary black holes with χ_{eff} negative and inconsistent with zero. This would require not only highly anti-aligned spins, but also significant spin magnitudes of merging BHs. While isolated evolution can produce strong spin-orbit misalignment and some instances where $\chi_{\text{eff}} < 0$, an inferred population of binary black holes with comparable proportions of large positive and large negative χ_{eff} would be more difficult to explain within our model. A more systematic study of the statistical properties of spin alignment in isolated binary evolution is necessary. Ongoing work on this topic will be presented elsewhere (Gerosa et al. 2017, in prep.).

Our predictions result from simple, in part uncertain, but standard, single and binary evolution calculations. Therefore, it is encouraging that thus far LIGO observations seem to confirm our theoretical predictions of BH masses and merger rates (Belczynski et al. 2010b,a; Dominik et al. 2015; Belczynski et al. 2016c,b). Our model makes several other easily verifiable predictions. As in prior work, due to pair-instability pulsation and supernova effects, we predict the absence of BHs with masses between $\approx 55\text{--}135 M_{\odot}$ (Belczynski et al. 2016a). And in this study we predict that heavy black holes will be slowly spinning.

Acknowledgements. We appreciate pointers and comments from Selma de Mink, Enrico Ramirez-Ruiz, Ilya Mandel, Cole Miller, Thomas Janka, Serena Repetto and Simon Stevenson. We would like to thank thousands of Universe@home users that have provided their personal computers and phones for our simulations, and in particular to Krzysztof Piszczek and Grzegorz Wiktorowicz (program IT and science managers). KB acknowledges support from the Polish National Science Center (NCN) grants: Sonata Bis 2 (DEC-2012/07/E/ST9/01360), OPUS (2015/19/B/ST9/03188) and MAESTRO (2015/18/A/ST9/00746); KB and JPL of the grant OPUS (2015/19/B/ST9/01099). DG is supported by NASA through Einstein Postdoctoral Fellowship Grant No. PF6-170152 awarded by the Chandra X-ray Center, which is operated by the Smithsonian Astrophysical Observatory for NASA under contract NAS8-03060. TB acknowledges support from the Polish National Science Center (NCN) Grant No. UMO-2014/14/M/ST9/00707. EB is supported by NSF Grants No. PHY-1607130, AST-1716715, and by FCT contract IF/00797/2014/CP1214/CT0012 under the IF2014 Programme. C.G., G.M., and S.E. acknowledge support from the Swiss National Science Foundation (project number 200020-160119). ROS is supported by NSF AST-1412449, PHY-1505629, and PHY-1607520. DAB acknowledges support from National Science Foundation Grant No. PHY-1404395. KB, CLF, DAB, GM, JPL are supported in part by the National Science Foundation under Grant No. NSF PHY-1125915 (to KITP, UC Santa Barbara). JPL was supported by a grant from the French Space Agency CNES.

References

- Abbott, B. P., Abbott, R., Abbott, T. D., et al. 2016a, *Physical Review X*, 6, 041015
- Abbott, B. P., Abbott, R., Abbott, T. D., et al. 2016b, *ApJ*, 818, L22
- Abbott, B. P. et al. 2016c, *Physical Review Letters*, 116, 241103
- Abbott, B. P. et al. 2016d, *Physical Review Letters*, 116, 061102
- Abbott, B. P. et al. 2017a, <http://www.ligo.org/news/index.php>, June 2017 update on LIGO's second observing run
- Abbott, B. P. et al. 2017b, *Phys. Rev. Lett.*, 118, 221101
- Albrecht, S., Winn, J. N., Torres, G., et al. 2014, *ApJ*, 785, 83
- Askar, A., Szkudlarek, M., Gondek-Rosińska, D., Giersz, M., & Bulik, T. 2017, *MNRAS*, 464, L36
- Bae, Y.-B., Kim, C., & Lee, H. M. 2014, *MNRAS*, 440, 2714
- Bahramian, A., Heinke, C. O., Tudor, V., et al. 2017, *MNRAS*, 467, 2199
- Belczynski, K., Bulik, T., Fryer, C. L., et al. 2010a, *ApJ*, 714, 1217
- Belczynski, K., Buonanno, A., Cantiello, M., et al. 2014, *ApJ*, 789, 120
- Belczynski, K., Dominik, M., Bulik, T., et al. 2010b, *ApJ*, 715, L138
- Belczynski, K., Heger, A., Gladysz, W., et al. 2016a, *A&A*, 594, A97
- Belczynski, K., Holz, D. E., Bulik, T., & O'Shaughnessy, R. 2016b, *Nature*, 534, 512

³ The estimated masses and spins of these systems can be found online at <https://stellarcollapse.org>

- Belczynski, K., Kalogera, V., & Bulik, T. 2002, *ApJ*, 572, 407
- Belczynski, K., Kalogera, V., Rasio, F. A., et al. 2008, *ApJS*, 174, 223
- Belczynski, K., Repetto, S., Holz, D. E., et al. 2016c, *ApJ*, 819, 108
- Belczynski, K., Ryu, T., Perna, R., et al. 2016d, *ArXiv e-prints* [arXiv:1612.01524]
- Belczynski, K., Wiktorowicz, G., Fryer, C. L., Holz, D. E., & Kalogera, V. 2012, *ApJ*, 757, 91
- Benacquista, M. J. & Downing, J. M. B. 2013, *Living Reviews in Relativity*, 16, 4
- Casares, J. & Jonker, P. G. 2014, *Space Sci. Rev.*, 183, 223
- Chatterjee, S., Fregeau, J. M., Umbreit, S., & Rasio, F. A. 2010, *ApJ*, 719, 915
- Chomiuk, L., Strader, J., Maccarone, T. J., et al. 2013, *ApJ*, 777, 69
- Corral-Santana, J. M., Casares, J., Muñoz-Darias, T., et al. 2016, *A&A*, 587, A61
- de Mink, S. E. & Belczynski, K. 2015, *ApJ*, 814, 58
- de Mink, S. E. & Mandel, I. 2016, *MNRAS*, 460, 3545
- Dewi, J. D. M. & Tauris, T. M. 2000, *A&A*, 360, 1043
- Dominik, M., Belczynski, K., Fryer, C., et al. 2012, *ApJ*, 759, 52
- Dominik, M., Berti, E., O'Shaughnessy, R., et al. 2015, *ApJ*, 806, 263
- Downing, J. M. B., Benacquista, M. J., Giersz, M., & Spurzem, R. 2010, *MNRAS*, 407, 1946
- Eggenberger, P., Montalbán, J., & Miglio, A. 2012, *A&A*, 544, L4
- Ekström, S., Georgy, C., Eggenberger, P., et al. 2012, *A&A*, 537, A146
- Eldridge, J. J. & Stanway, E. R. 2016, *MNRAS*, 462, 3302
- Elmegreen, B. G. 2010, *ApJ*, 712, L184
- Eroshenko, Y. N. 2016, *ArXiv e-prints* [arXiv:1604.04932]
- Farr, W. M., Stevenson, S., Miller, M. C., et al. 2017, *ArXiv e-prints* [arXiv:1706.01385]
- Fishbach, M., Holz, D. E., & Farr, B. 2017, *ApJ*, 840, L24
- Fryer, C. L., Belczynski, K., Wiktorowicz, G., et al. 2012, *ApJ*, 749, 91
- Fryer, C. L. & Heger, A. 2000, *ApJ*, 541, 1033
- Fryer, C. L. & Kusenko, A. 2006, *ApJS*, 163, 335
- Fryer, C. L., Woosley, S. E., & Heger, A. 2001, *ApJ*, 550, 372
- Georgy, C., Ekström, S., Eggenberger, P., et al. 2013, *A&A*, 558, A103
- Georgy, C., Ekström, S., Meynet, G., et al. 2012, *A&A*, 542, A29
- Gerosa, D. & Berti, E. 2017, *ArXiv e-prints* [arXiv:1703.06223]
- Gerosa, D., Kesden, M., Berti, E., O'Shaughnessy, R., & Sperhake, U. 2013, *Phys. Rev. D*, 87, 104028
- Gerosa, D., Kesden, M., Sperhake, U., Berti, E., & O'Shaughnessy, R. 2015, *Phys. Rev. D*, 92, 064016
- Giersz, M., Hoggie, D. C., Hurley, J. R., & Hypki, A. 2013, *MNRAS*, 431, 2184
- González Hernández, J. I., Casares, J., Rebolo, R., et al. 2011, *ApJ*, 738, 95
- González Hernández, J. I., Rebolo, R., & Israelian, G. 2008, *A&A*, 478, 203
- González Hernández, J. I., Rebolo, R., Israelian, G., et al. 2004, *ApJ*, 609, 988
- González Hernández, J. I., Rebolo, R., Israelian, G., et al. 2006, *ApJ*, 644, L49
- Gou, L., McClintock, J. E., Liu, J., et al. 2009, *ApJ*, 701, 1076
- Gou, L., McClintock, J. E., Remillard, R. A., et al. 2014, *ApJ*, 790, 29
- Green, A. M. 2017, *ArXiv e-prints* [arXiv:1705.10818]
- Harris, W. E. 1996, *AJ*, 112, 1487
- Heger, A. & Woosley, S. E. 2002, *ApJ*, 567, 532
- Hobbs, G., Lorimer, D. R., Lyne, A. G., & Kramer, M. 2005, *MNRAS*, 360, 974
- Hotokezaka, K. & Piran, T. 2017, *ArXiv e-prints* [arXiv:1702.03952]
- Hurley, J. R., Pols, O. R., & Tout, C. A. 2000, *MNRAS*, 315, 543
- Hurley, J. R., Sippel, A. C., Tout, C. A., & Aarseth, S. J. 2016, *PASA*, 33, e036
- Israelian, G., Rebolo, R., Basri, G., Casares, J., & Martín, E. L. 1999, *Nature*, 401, 142
- Kalogera, V. 2000, *ApJ*, 541, 319
- Katz, H. & Ricotti, M. 2013, *MNRAS*, 432, 3250
- Kinugawa, T., Inayoshi, K., Hotokezaka, K., Nakauchi, D., & Nakamura, T. 2014, *MNRAS*, 442, 2963
- Kinugawa, T., Nakamura, T., & Nakano, H. 2016, *ArXiv e-prints* [arXiv:1610.00305]
- Kravtsov, A. V. & Gnedin, O. Y. 2005, *ApJ*, 623, 650
- Kruckow, M. U., Tauris, T. M., Langer, N., et al. 2016, *A&A*, 596, A58
- Kruijssen, J. M. D. 2012, *MNRAS*, 426, 3008
- Kruijssen, J. M. D. & Mieske, S. 2009, *A&A*, 500, 785
- Kusenko, A. & Segrè, G. 1996, *Physical Review Letters*, 77, 4872
- Kushnir, D., Zaldarriaga, M., Kollmeier, J. A., & Waldman, R. 2016, *MNRAS*, 462, 844
- Lai, D. & Qian, Y.-Z. 1998, *ApJ*, 495, L103
- Lipunov, V. M., Postnov, K. A., & Prokhorov, M. E. 1997, *Astronomy Letters*, 23, 492
- Liu, J., McClintock, J. E., Narayan, R., Davis, S. W., & Orosz, J. A. 2010, *ApJ*, 719, L109
- Loveridge, A. J., van der Sluis, M. V., & Kalogera, V. 2011, *ApJ*, 743, 49
- MacLeod, M., Antoni, A., Murguia-Berthier, A., Macias, P., & Ramirez-Ruiz, E. 2017, *ApJ*, 838, 56
- MacLeod, M. & Ramirez-Ruiz, E. 2015a, *ApJ*, 803, 41
- MacLeod, M. & Ramirez-Ruiz, E. 2015b, *ApJ*, 798, L19
- Madau, P. & Dickinson, M. 2014, *ARA&A*, 52, 415
- Mandel, I. 2016, *MNRAS*, 456, 578
- Mapelli, M. 2016, *MNRAS*, 459, 3432
- Mapelli, M., Colpi, M., & Zampieri, L. 2009, *MNRAS*, 395, L71
- Marchant, P., Langer, N., Podsiadlowski, P., Tauris, T. M., & Moriya, T. J. 2016, *A&A*, 588, A50
- Marks, M., Kroupa, P., Dabringhausen, J., & Pawlowski, M. S. 2012, *MNRAS*, 422, 2246
- Mennekens, N. & Vanbeveren, D. 2014, *A&A*, 564, A134
- Meurs, E. J. A. & van den Heuvel, E. P. J. 1989, *A&A*, 226, 88
- Meynet, G., Chomienne, V., Ekström, S., et al. 2015, *A&A*, 575, A60
- Murguia-Berthier, A., MacLeod, M., Ramirez-Ruiz, E., Antoni, A., & Macias, P. 2017, *ArXiv e-prints* [arXiv:1705.04698]
- Murray, J. R., Chakrabarty, D., Wynn, G. A., & Kramer, L. 2002, *MNRAS*, 335, 247
- Nelemans, G., Yungelson, L. R., & Portegies Zwart, S. F. 2001, *A&A*, 375, 890
- O'Leary, R. M., O'Shaughnessy, R., & Rasio, F. A. 2007, *Phys. Rev. D*, 76, 061504
- Orosz, J. A., Kuulkers, E., van der Klis, M., et al. 2001, *ApJ*, 555, 489
- O'Shaughnessy, R., Gerosa, D., & Wysocki, D. 2017, *ArXiv e-prints* [arXiv:1704.03879]
- Ott, C. D., Burrows, A., Thompson, T. A., Livne, E., & Walder, R. 2006, *ApJS*, 164, 130
- Packet, W. 1981, *A&A*, 102, 17
- Pavlovskii, K., Ivanova, N., Belczynski, K., & Van, K. X. 2017, *MNRAS*, 465, 2092
- Paxton, B., Marchant, P., Schwab, J., et al. 2015, *ApJS*, 220, 15
- Podsiadlowski, P., Rappaport, S., & Han, Z. 2003, *MNRAS*, 341, 385
- Portegies Zwart, S. F., Baumgardt, H., Hut, P., Makino, J., & McMillan, S. L. W. 2004, *Nature*, 428, 724
- Postnov, K. & Kuranov, A. 2017, *ArXiv e-prints* [arXiv:1706.00369]
- Racine, É. 2008, *Phys. Rev. D*, 78, 044021
- Repetto, S., Igoshev, A. P., & Nelemans, G. 2017, *MNRAS*, 467, 298
- Repetto, S. & Nelemans, G. 2015, *MNRAS*, 453, 3341
- Ricker, P. M. & Taam, R. E. 2008, *ApJ*, 672, L41
- Rodriguez, C. L., Chatterjee, S., & Rasio, F. A. 2016a, *Phys. Rev. D*, 93, 084029
- Rodriguez, C. L., Haster, C.-J., Chatterjee, S., Kalogera, V., & Rasio, F. A. 2016b, *ApJ*, 824, L8
- Rodriguez, C. L., Zevin, M., Pankow, C., Kalogera, V., & Rasio, F. A. 2016c, *ApJ*, 832, L2
- Sadowski, A., Belczynski, K., Bulik, T., et al. 2008, *ApJ*, 676, 1162
- Sana, H., de Mink, S. E., de Koter, A., et al. 2012, *Science*, 337, 444
- Santamaría, L., Ohme, F., Ajith, P., et al. 2010, *Phys. Rev. D*, 82, 064016
- Sasaki, M., Suyama, T., Tanaka, T., & Yokoyama, S. 2016, *ArXiv e-prints* [arXiv:1603.08338]
- Socrates, A., Blaes, O., Hungerford, A., & Fryer, C. L. 2005, *ApJ*, 632, 531
- Spera, M., Mapelli, M., & Bressan, A. 2015, *MNRAS*, 451, 4086
- Spruit, H. C. 1999, *A&A*, 349, 189
- Spruit, H. C. 2002, *A&A*, 381, 923
- Stevenson, S., Vigna-Gómez, A., Mandel, I., et al. 2017, *Nature Communications*, 8, 14906
- Strader, J., Chomiuk, L., Maccarone, T. J., Miller-Jones, J. C. A., & Seth, A. C. 2012, *Nature*, 490, 71
- Tamborra, I., Hanke, F., Janka, H.-T., et al. 2014, *Astrophys. J.*, 792, 96
- Tauris, T. M. & Dewi, J. D. M. 2001, *A&A*, 369, 170
- Tetarenko, B. E., Bahramian, A., Arnason, R. M., et al. 2016, *ApJ*, 825, 10
- Tutukov, A. V. & Yungelson, L. R. 1993, *MNRAS*, 260, 675
- Villante, F. L., Serenelli, A. M., Delahaye, F., & Pinsonneault, M. H. 2014, *ApJ*, 787, 13
- Vink, J. S., de Koter, A., & Lamers, H. J. G. L. M. 2001, *A&A*, 369, 574
- Voss, R. & Tauris, T. M. 2003, *MNRAS*, 342, 1169
- Webb, J. J. & Leigh, N. W. C. 2015, *MNRAS*, 453, 3278
- Woosley, S. E. 2017, *ApJ*, 836, 244
- Woosley, S. E. & Heger, A. 2015, in *Astrophysics and Space Science Library*, Vol. 412, *Very Massive Stars in the Local Universe*, ed. J. S. Vink, 199
- Xu, X.-J. & Li, X.-D. 2010, *ApJ*, 722, 1985
- Zahn, J.-P. 1992, *A&A*, 265, 115
- Zaldarriaga, M., Kushnir, D., & Kollmeier, J. A. 2017, *ArXiv e-prints* [arXiv:1702.00885]
- Zampieri, L. & Roberts, T. P. 2009, *MNRAS*, 400, 677

Appendix A: Making GW170104

Figure 2 shows the formation and evolution of a typical binary which results in a BH-BH merger with similar properties to GW170104. The progenitor binary was formed ~ 9.1 Gyr ago ($z \sim 1.45$) in a low-metallicity environment $Z = 0.0007$ ($0.035 Z_{\odot}$) as a pair of two MS stars with masses of $85 M_{\odot}$ and $60 M_{\odot}$ on a wide orbit with the pericenter distance of $\sim 1000 R_{\odot}$. As the primary ends its MS evolution and rapidly expands as a Hertzsprung gap (HG) star it initiates a stable case-B mass transfer. In our M20 model (see Sec. 2.3 for details) we assume that 20% of the mass is accreted by the MS companion, while the other 80% is lost from the system. During mass transfer the primary is stripped of its almost entire H-rich envelope and becomes a naked helium WR star with the mass of $37 M_{\odot}$. Only 0.3 Myr later it finishes its nuclear evolution and forms a BH ($M_{\text{BH1}} = 30.3 M_{\odot}$) in a direct collapse event (no natal kick), losing 10% of its mass in neutrino emission. The mass of the CO core of the BH progenitor is $M_{\text{CO}} = 27.1 M_{\odot}$, which means that the first BH is assigned with zero initial spin ($a_{\text{spin1}} = 0.0$, see Sec. 2.2).

The companion, on the other hand, has increased its mass during the mass transfer up to $67 M_{\odot}$. It has also been rejuvenated (which we model according to eq. 58 of Belczynski et al. (2008)) and spun up and at the offset of mass transfer is about 70% of its way through the MS phase. During the HG stage it expands up to $700 R_{\odot}$, which is, however, not enough to cause a RLOF. It further increases its radius up to $880 R_{\odot}$ as a core-helium-burning supergiant, at which point it initiates a dynamically unstable mass transfer and the CE phase. As a result the wide binary orbit ($a = 2000 R_{\odot}$) has decayed down to $a = 34 R_{\odot}$ and the secondary is left without any envelope as a naked WR star. We assume a 5% Bondi-Hoyle accretion rate onto a compact object during CE, which leads the first BH to an only slight increase of its mass (by $0.4 M_{\odot}$) and spin ($a_{\text{spin1}} = 0.042$). Shortly after (0.3 Myr after the CE) the secondary forms a BH in a direct collapse ($M_{\text{BH2}} = 23.8 M_{\odot}$) with no natal kick and only 10% neutrino mass loss. Because it has accreted a significant fraction of its mass ($\sim 20\%$) while still on the MS we assume that its increased rotation has led to a $\sim 20\%$ increase of the CO core mass with respect to the non-rotation stellar models (see Sec. 2.3). With the CO core mass of $M_{\text{CO}} = 24.9 M_{\odot}$ the second BH is assigned with initial spin of $a_{\text{spin2}} = 0.142$.

The BH-BH is formed after 5 Myr of binary evolution on a close ($a = 36.8 R_{\odot}$) and almost circular orbit ($e = 0.05$). The time to coalescence (emission of gravitational waves) is 6.9 Gyr. For this particular evolution/model we assume no natal kicks at the formation of direct massive BHs. It means that the BH spin vectors are most likely aligned with the binary angular momentum ($\Theta_1 = \Theta_2 = 0$ deg). This produces an upper limit on the effective spin parameter (see eq. 1). For this particular BH masses, their spins and spin tilts we obtain rather low effective spin of the BH-BH binary $\chi_{\text{eff}} = 0.086$. The progenitor binary forms at $z = 1.45$ (4.3 Gyr after Big Bang; close to a peak of star formation; $z \approx 2$), and BH-BH merger takes place at $z = 0.18$ (11.2 Gyr after Big Bang). All of the system properties are within 90% of credible level of the GW170104 (see Sec. 1).

Appendix B: The Effective Spin Parameter: χ_{eff}

The Bayesian analysis reported in Abbott et al. (2017b) adopts prior assumptions about the relative likelihood of different spin magnitudes (uniform) and spin directions (isotropic). These assumptions are not suitable for comparison to the binary evolution

model we adopt, which as presented here requires both individual spins to be aligned and therefore $\chi_{\text{eff}} < 0$.

Within the context of our model, we therefore reassess the reported limit, concluding $\chi_{\text{eff}} < 0.2$ at approximately 90% confidence, in the context of our model.

We can justify this reanalysis using only the reported LIGO result on χ_{eff} , restricted to $\chi_{\text{eff}} > 0$. Approximating the LIGO distribution as nearly normal with mean $\mu = -0.21$ and width $\sigma_{\chi} \simeq 0.155$, we construct a truncated normal distribution $\propto \theta(\chi) \exp -(\chi + \mu)^2 / 2\sigma^2$, which has a 90% upper limit at $x \simeq 0.2$.

We arrive at a similar result by reanalyzing the underlying LIGO data using the same model and techniques (including the prior), then restricting to configurations with two positive $\chi_{1,z}, \chi_{2,z} > 0$. Our revised upper limit is consistent with the range of plausible χ_{eff} , as reported by LIGO (Figure 5, supplementary material), corresponding to approximately a 98–99% confidence limit within the strong assumptions of their original analysis.

Appendix C: Globular cluster BH-BH merger rates

The predicted local rate density of coalescing BH-BH binaries depends on the particular formation scenario which is assumed. In general, all formation scenarios start with an underlying stellar population that has some associated star formation rate (SFR)⁴, and we assume that we know the SFR as a function of redshift. Each scenario provides a recipe for the fraction of the initial stellar mass which leads to the formation of BH-BH binary mergers. Black holes form almost immediately (\sim few Myr) after the formation of the massive progenitor stars. After the BH-BH binaries are formed, there is a delay time as they slowly inspiral due to the emission of gravitational-waves, eventually resulting in a merger. Delay time distribution can be steeper in GCs as contrasted with isolated BH-BH formation, as some dynamical interactions may harden already close BH-BH binaries, and some may disrupt wide BH-BH binaries. The distribution of delay times depends on the particular formation model of the merging BH-BH binaries. If the distribution of the semimajor axes of the newly formed BH-BH binaries can be described by a power law $dN/da \approx a^{-\beta}$, then the distribution of the merger times is $dN/dt \approx t^{-\alpha}$, where $\alpha = (3 + \beta)/4$, since the merger times is proportional to $t \propto a^4$. We are only interested in the models where there is a wide range of semi-major axes, and a wide range of merger times. If the range is narrow, which corresponds to large β than all mergers happen at roughly the same time. If the formation process is scale independent for some range of semimajor axes than $\beta = 1$. In fact such distributions are obtained in the GC simulations by Askar et al. (2017). Rodriguez et al. (2016a) does not present the delay time distribution however the merger events as a function of redshift in their Fig.2 correspond to roughly uniform distribution of mergers over redshift, consistent with the detailed simulations by Askar et al. (2017). One can see that even if β varies in an extreme range from 0 to 7 than α is between 0.75 and 2, thus for most astrophysical scenarios is constrained to $1 < \alpha < 2$.

A useful quantity to summarize the binary formation process is the compact object binary formation efficiency, defined as the number of merging BH-BH binaries formed per unit of star forming mass. This has a maximum value in the extreme case where all the black holes that formed in a given environment end up in merging BH-BH binaries. For the Salpeter initial

⁴ An exception to this would be a primordial black hole formation scenario. Given observational constraints and theoretical challenges associated with these models, we neglect them in this work.

mass function this maximum is $f_{\text{MAX}} = 1.8 \times 10^{-3} M_{\odot}^{-1}$, assuming that all stars with the mass above $20 M_{\odot}$ form black holes. This number becomes slightly smaller if we assume that the initial population contains some binaries.

For the case of globular clusters (GCs), we know that the total stellar mass in GCs in the Milky Way is roughly 0.1%. The mass of the GCs in the Milky Way can be estimated using the GC catalog (Harris 1996) and using the measured value of the mass to light ratio of $\approx M_{\odot}/L_{\odot}$ (Kruijssen & Mieske 2009), to obtain the mass of $\approx 3 \times 10^7 M_{\odot}$. Thus the mass of observed GCs in the Milky Way is 10^{-4} of the total mass of the Galaxy. Cosmological GC formation simulations show that this fraction can be close to 0.01% (Kravtsov & Gnedin 2005). However, small GCs may have dissolved and large GCs may have lost some mass, while GCs close to the Galactic center may quickly migrate to the center due to dynamical friction. Most of low mass GCs close to the Galactic center are quickly dissolved, and about 60–70% of the cluster mass will be lost during the Hubble time of dynamical evolution (Chatterjee et al. 2010; Giersz et al. 2013). Thus the total fraction of stellar mass processed in GCs was larger; perhaps about 1% and certainly no more than 10% of the mass in the field.

The GC star formation rate (GCSFR) is difficult to measure. Katz & Ricotti (2013) present a model where the GCSFR peaks at $z \sim 2$, and decreases to almost 0 for redshifts $z \lesssim 1.5$. This allows to calculate the local ($z \approx 0$) BH-BH merger rate density from the GCs assuming that all GCs formed at one epoch:

$$\mathcal{R} = \left(\int \text{GCSFR}(z) dt \right) \times f_{\text{BHBH}} \times \frac{dN}{dt}(t_{\text{del}}) \frac{1}{1 + z(t_{\text{del}})} \quad (\text{C.1})$$

where f_{BHBH} is the BH-BH formation efficiency in GCs, $\frac{dN}{dt}$ is the delay time distribution, and t_{del} is the time since the peak of GCSFR. The first factor is roughly 0.01–0.1 of the total SFR in the field. Using the results of Askar et al. (2017) we adopt the largest value in this study $f_{\text{BHBH}} \approx 0.05 f_{\text{MAX}}$, while for the binaries in the field it is $\approx 0.01 f_{\text{MAX}}$ (depending on metallicity). Rodriguez et al. (2016a) obtain the value of $f_{\text{BHBH}} \approx 0.10$ – $0.20 f_{\text{MAX}}$, for the cluster masses from $10^5 M_{\odot}$ to $4 \times 10^5 M_{\odot}$.

Finally, the delay time distribution can be approximated by a power-law (see Fig.3 in Askar et al. (2017)):

$$\frac{dN}{dt} \approx \frac{0.15^{-1}}{t}, \quad (\text{C.2})$$

for time delays above 0.1 Gyr; for a typical delay time of $t_{\text{del}} = 6$ Gyr, it is $dN/dt \approx 2.5 \times 10^{-11} \text{yr}^{-1}$. The integral over the star formation from Katz & Ricotti (2013) yields

$$\int \text{GCSFR} dt \approx 2 \times 10^7 M_{\odot} \text{Mpc}^{-3}, \quad (\text{C.3})$$

leading to a rate estimate of

$$\begin{aligned} \mathcal{R}_{\text{GC}} &\approx 2 \times 10^7 M_{\odot} \text{Mpc}^{-3} \times 0.05 f_{\text{MAX}} \times 2.5 \times 10^{-11} \text{yr}^{-1} \times \frac{1}{3} \\ &\approx 15 \text{Gpc}^{-3} \text{yr}^{-1}. \end{aligned} \quad (\text{C.4})$$

This rate is rather optimistic, as we have adopted the highest GCSFR available in Katz & Ricotti (2013) and the highest BH-BH formation efficiency from the largest suite of theoretical models presented in Askar et al. (2017). This overall estimate is broadly consistent with the recent theoretical BH-BH merger rate estimates in GC: $5 \text{Gpc}^{-3} \text{yr}^{-1}$ (Rodriguez et al. 2016a) and

$5.4 \text{Gpc}^{-3} \text{yr}^{-1}$ (Askar et al. 2017). Additionally, Askar et al. (2017) estimated that uncertainties in the maximum initial mass of a GC, the maximum initial mass of a star in a GC or not well constrained IMF of stars in GC can allow for BH-BH merger rates as high as $\lesssim 30 \text{Gpc}^{-3} \text{yr}^{-1}$. In conclusion, the rate density of GC BH-BH mergers is uncertain (see below), but nonetheless much smaller than the rates allowed by field binary evolution (see Tab. 2).

There are many factors that can change the merger rates for BH-BH binaries that originate from GCs. The GCSFR is poorly constrained. If more stars were born in dense systems like GCs then this would increase the rate of dynamically formed BH-BH binaries. Theoretical estimates for the fraction of all star formation that occurs in (open and globular) bound stellar clusters indicate that 30–35% of all stars may have once formed in bound stellar clusters (Kruijssen 2012). However, given that many more open clusters are observed compared to GCs, a significant fraction of these bound stellar clusters should be open clusters. Even if about 10% of all bound stellar clusters are GCs, the amount of star formation in GCs will not exceed 3.5%. It has been shown by (Rodriguez et al. 2016a) and Askar et al. (2017) that regardless of metallicity, more massive GCs produce more coalescing BH-BH binaries compared to lower mass GCs. There is significant uncertainty as to how massive GCs were at the time of their birth: ~ 5 – 10 times initially more massive than their currently observed masses (Webb & Leigh 2015). However, most GC clusters are expected to have low mass (GC mass function falls-off as a steep power-law with index of -2 ; Elmegreen (2010)). The maximum initial mass for the stars in GC is also uncertain and if the IMF is sampled with a larger or smaller maximum initial mass then there will be more or less BH progenitors in the GC that could go on to potentially form BH-BH binaries. Since, there is some evidence that the IMF is top-heavy in dense low metallicity environments like GCs (Marks et al. 2012) this may potentially increase the total number of BH progenitors in GCs. The low-redshift merger rate may change both ways depending on the delay to merger time distribution of the BH-BH formed in globular clusters. The most massive stars may get ejected from clusters through dynamical interactions even before forming BHs and BHs may be removed from clusters if they receive significant natal kicks ($\gtrsim 100$ – 200km s^{-1} ; see § 2.3 for the discussion) reducing the GC BH-BH merger rates.

Appendix D: BH mass and natal kicks in StarTrack

For models M10 and M20 in this work we assume what we refer to as “fallback-decreased” BH natal kicks, or low-to-zero BH natal kicks set by fallback (see Tab. 1). More specifically, we adopt prescriptions for the compact remnant masses and birth velocities from Fryer et al. (2012), choosing their “Rapid” supernova mechanism that is able to reproduce the observed mass-gap between NSs and BHs (Belczynski et al. 2012). Here we briefly summarize the adopted model.

On formation, each BH is assigned a randomly oriented natal kick velocity with the magnitude calculated as:

$$V_{\text{NK}} = (1 - f_{\text{fb}}) \sqrt{V_x^2 + V_y^2 + V_z^2}, \quad (\text{D.1})$$

where V_x , V_y , V_z are three velocity components drawn from a Maxwellian distribution with $\sigma = 265 \text{km s}^{-1}$ (Hobbs et al. 2005), and f_{fb} is a fallback parameter standing for the fraction of the stellar envelope that falls back onto the proto-compact object (i.e., $f_{\text{fb}} = 1$ is a direct BH formation). Specifically, the mass

of the forming BH is calculated as:

$$M_{\text{BH}} = 0.9 [M_{\text{proto}} + f_{\text{fb}}(M - M_{\text{proto}})] , \quad (\text{D.2})$$

where $M_{\text{proto}} = 1.0 M_{\odot}$ is the proto-compact object mass, M is the pre-supernova mass of the star and the factor 0.9 accounts for the 10% baryonic mass loss in neutrino emission.

In models M13, M23, M25 and M26, we do not reduce the BH natal kicks because of the fallback (i.e., $f_{\text{fb}} = 0$ in eq. D.1) and we set the value of σ to 265 km s^{-1} (M13 and M23), to 130 km s^{-1} (M25) or to 70 km s^{-1} (M26). Note that the BH masses are calculate following eq. D.2 in all our models.

The combination of eq. D.1 and eq. D.2 in models M10 and M20 results in a correlation that more massive BHs tend to receive smaller kick velocities. This agrees with the natural intuition of momentum conservation. However, mass-independent natal kicks (as assumed in models M13, M23, M25 and M26) are also considered in our study (see § 2.3 for discussion).

The fraction of matter falling back (f_{fb}) is the key parameter of this model. We calculate it based only on the final CO core mass M_{CO} of the star:

$$f_{\text{fb}} = \begin{cases} 1.0, & \text{for } 6.0 \leq M_{\text{CO}} \leq 7.0 M_{\odot} \\ a_1 M_{\text{CO}} + b_1, & \text{for } 7.0 \leq M_{\text{CO}} \leq 11.0 M_{\odot} \\ 1.0, & \text{for } M_{\text{CO}} \geq 11.0 M_{\odot} \end{cases} \quad (\text{D.3})$$

with $a_1 = 0.25 - \frac{1.275}{M - M_{\text{proto}}}^5$ and $b_1 = -11a_1 + 1$. Stars with less massive CO cores (than listed in the above formula) form neutron stars with $M_{\text{NS}} \in [1.2, 2.2] M_{\odot}$ (see Eq. 16 of Fryer et al. (2012)).

In practice, most of our BHs in BH-BH mergers detectable with the O1/O2 LIGO were formed in a direct collapse ($f_{\text{fb}} = 1$): 89% of all the BHs in model M10 and even more, 91%, in model M20 (due to an additionally assumed 20% increase of M_{CO} for mass accreting, low metallicity stars, see § 2.3).

The relation between the BH mass at formation and the final CO core mass of its progenitor in our simulations is set by the combination of eq. D.2 and eq. D.3, together with the pre-supernova mass of the star. In Fig. D.1 we show $M_{\text{CO}}-M_{\text{BH}}$ relation for model M20 and BH-BH mergers detectable with the O1/O2 LIGO. Note that even though we plot M_{BH} at the moment of the BH formation, it is very similar to the final BH mass (see Sec. 3.3).

For low mass BHs ($5 \lesssim M_{\text{BH}} \lesssim 20 M_{\odot}$) the relation between M_{CO} and M_{BH} shows complicated behavior due to the effect of wind mass loss (this is the regime in which winds can remove entire stellar envelope and in which LBV winds can turn on) and due to transitions between partial fallback and direct BH formation. For massive BHs ($20 \lesssim M_{\text{BH}} \lesssim 40 M_{\odot}$) the relation is nearly linear. This is because the massive progenitors of these BHs are WR stars with CO core masses similar to entire progenitor masses. Since in these mass regime we expect a direct collapse to a BH, a BH mass is almost equal to a CO core mass. For the most massive BHs ($M_{\text{BH}} \gtrsim 40 M_{\odot}$) the BH mass does not increase with CO core mass as pulsation pair-instability supernovae remove the outer stellar layers. This occurs for the CO core masses larger than $\sim 37.5 M_{\odot}$ as seen in Fig. D.1 and corresponds to stars that have their helium cores in mass range $M_{\text{He}} = 45-65 M_{\odot}$. Stars with even more massive cores ($M_{\text{He}} > 65 M_{\odot}$, or $M_{\text{CO}} > 55 M_{\odot}$) are entirely disrupted in the pair-instability supernovae. Details of our assumptions on pair-instability supernovae are given in Belczynski et al. (2016a).

⁵ Note that this is the correct formula for a_1 , the equation given in the ApJ published version of Fryer et al. (2012) has a typo.

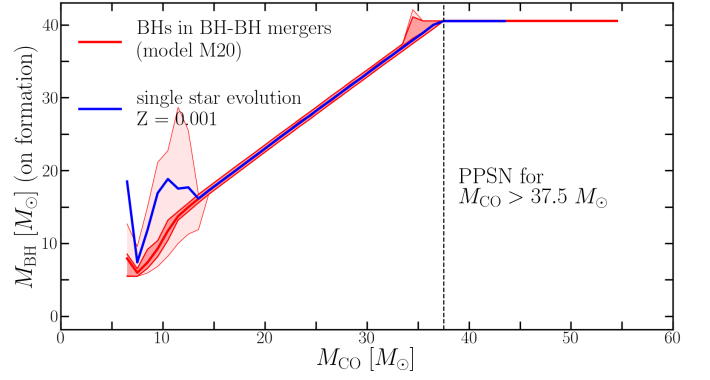


Fig. D.1. The relation between the BH progenitor star CO core mass and BH formation mass. In red we show all BHs that are components of the BH-BH mergers that are detectable with the LIGO O1/O2 in our model M20. The light red shaded area marks all the BHs (100%), the darker red marks typical BH progenitors (vast majority: 98%), while the central red curve is the average BH mass for a given CO core mass. For comparison, we also show (blue) this relation for single star evolution at low-metallicity ($Z = 0.001$; typical of massive BH-BH progenitors).

Fig. D.1 can be used in combination with eq. 4 to see that we predict zero initial BH spins (i.e. when $M_{\text{CO}} > 27 M_{\odot}$) for heavy BHs of about $M_{\text{BH}} \gtrsim 30 M_{\odot}$.